



Chinese Pharmaceutical Association
Institute of Materia Medica, Chinese Academy of Medical Sciences

Acta Pharmaceutica Sinica B

www.elsevier.com/locate/apsb
www.sciencedirect.com



ORIGINAL ARTICLE

Design, synthesis, and biological evaluation of quinazolin-4(3*H*)-one derivatives co-targeting poly(ADP-ribose) polymerase-1 and bromodomain containing protein 4 for breast cancer therapy



Xiaosa Chang[†], Dejuan Sun[†], Danfeng Shi[†], Guan Wang,
Yanmei Chen, Kai Zhang, Huidan Tan, Jie Liu*, Bo Liu*,
Liang Ouyang*

State Key Laboratory of Biotherapy and Cancer Center, West China Hospital, Collaborative Innovation Center of Biotherapy, Sichuan University, Chengdu 610041, China

Received 27 February 2020; received in revised form 8 May 2020; accepted 28 May 2020

KEY WORDS

BRD4;
PARP1;
Dual-target inhibitor;
Synthetic lethality;
Quinazolin-4(3*H*)-one

Abstract This study was aimed to design the first dual-target small-molecule inhibitor co-targeting poly (ADP-ribose) polymerase-1 (PARP1) and bromodomain containing protein 4 (BRD4), which had important cross relation in the global network of breast cancer, reflecting the synthetic lethal effect. A series of new BRD4 and PARP1 dual-target inhibitors were discovered and synthesized by fragment-based combinatorial screening and activity assays that together led to the chemical optimization. Among these compounds, **19d** was selected and exhibited micromole enzymatic potencies against BRD4 and

Abbreviations: BC, breast cancer; BET, bromodomain and extra-terminal domain; *BRCA1/2*, breast cancer susceptibility gene 1/2; BRD4, bromodomain 4; CDK4/6, cyclin-dependent kinase 4/6; DSB, DNA double-strand break; EGFR, epidermal growth factor receptor; ELISA, enzyme linked immunosorbent assay; ER, estrogen receptor; ESI-HR-MS, high-resolution mass spectra; FDA, U.S. Food and Drug Administration; FITC, fluorescein isothiocyanate isomer I; HE, hematoxylin-eosin; HPLC, high-performance liquid chromatography; HR, homologous recombination; HRD, homologous recombination deficiency; IHC, immunohistochemistry; NHEJ, nonhomologous end-joining; PARP1, poly(ADP-ribose) polymerase-1; PI, propidium iodide; PK, pharmacokinetics; PPI, protein–protein interaction; SAR, structure–activity relationship; shRNA, short hairpin RNA; SOP, standard operation process; TCGA, the cancer genome atlas; TGI, tumor growth inhibition; TLC, thin-layer chromatography; TNBC, triple-negative breast cancer; TR-FRET, time-resolved fluorescence resonance energy transfer.

*Corresponding authors. Tel./fax: +86 28 85503817 (Jie Liu), +86 28 85164063 (Bo Liu), +86 28 85503817 (Liang Ouyang).

E-mail addresses: liujie2011@scu.edu.cn (Jie Liu), liubo2400@163.com (Bo Liu), ouyangliang@scu.edu.cn (Liang Ouyang).

[†]These authors made equal contributions to this work.

Peer review under responsibility of Institute of Materia Medica, Chinese Academy of Medical Sciences and Chinese Pharmaceutical Association

<https://doi.org/10.1016/j.apsb.2020.06.003>

2211-3835 © 2021 Chinese Pharmaceutical Association and Institute of Materia Medica, Chinese Academy of Medical Sciences. Production and hosting by Elsevier B.V. This is an open access article under the CC BY-NC-ND license (<http://creativecommons.org/licenses/by-nc-nd/4.0/>).

derivatives

PARP1, respectively. Compound **19d** was further shown to efficiently modulate the expression of BRD4 and PARP1. Subsequently, compound **19d** was found to induce breast cancer cell apoptosis and stimulate cell cycle arrest at G1 phase. Following pharmacokinetic studies, compound **19d** showed its antitumor activity in breast cancer susceptibility gene 1/2 (*BRCA1/2*) wild-type MDA-MB-468 and MCF-7 xenograft models without apparent toxicity and loss of body weight. These results together demonstrated that a highly potent dual-targeted inhibitor was successfully synthesized and indicated that co-targeting of BRD4 and PARP1 based on the concept of synthetic lethality would be a promising therapeutic strategy for breast cancer.

© 2021 Chinese Pharmaceutical Association and Institute of Materia Medica, Chinese Academy of Medical Sciences. Production and hosting by Elsevier B.V. This is an open access article under the CC BY-NC-ND license (<http://creativecommons.org/licenses/by-nc-nd/4.0/>).

1. Introduction

Breast cancer (BC) is a complex multigene disease and developed from the genetic defect or acquired DNA damage, and involves multiple cross-talks pathway, such as triple-negative breast cancer (TNBC) is more likely to carry *BRCA1/2* mutations, with high metastasis, recurrence rates and shorter overall survival rates^{1–4}. According to the statistics of international cancer research institute, breast cancer has become the highest incidence of cancer among women in the world⁵. Currently, the main treatment for BC patients is chemotherapy with small-molecule drugs in addition to radiotherapy and surgery^{6–8}. As shown in Fig. 1, such as neratinib, human epidermal growth factor receptor 2 (HER2) and epidermal growth factor receptor (EGFR) inhibitor; lapatinib, EGFR and receptor tyrosine-protein kinase ERBB-2 inhibitor; fulvestrant, estrogen receptor (ER) antagonist; exemestane, aromatase inhibitor; ribociclib and abemaciclib, cyclin-dependent kinase 4/6 (CDK4/6) inhibitors^{9–13}. These targeted therapy drugs have improved cancer treatment for many people in a certain period of time. However, to make further progress with genetically targeted cancer therapy, our

ability has been limited. Although partial responses to targeted therapies in selected patient populations are common, converting those partial responses to durable complete responses will require combination regimens that have been challenging to define^{14,15}. Until 2009, the first human clinical trial of poly (ADP-ribose) polymerase-1 (PARP1) inhibitor Olaparib confirmed the synthetic lethal effect of PARP1 inhibitor in the treatment of *BRCA1/2*-deficient breast cancer¹⁶. In the next 10 years, U.S. Food and Drug Administration (FDA) approved the antitumor drugs based on the concept of synthetic lethal for the treatment of ovarian cancer and breast cancer, as well as a lot of clinical research on pancreatic cancer and prostate cancer. PARP1 inhibitors (Fig. 1) have become the first clinically designed drugs base on synthesize lethal, and show great potential^{17–19}. Drug design method based on the concept of synthetic lethality may have broad potential to drive the discovery of the next wave of genetic cancer targets and ultimately the introduction of effective medicines that are still needed for most cancers^{20–22}.

Synthetic lethality, initially described in drosophila as recessive lethality, is classically defined as the setting in which

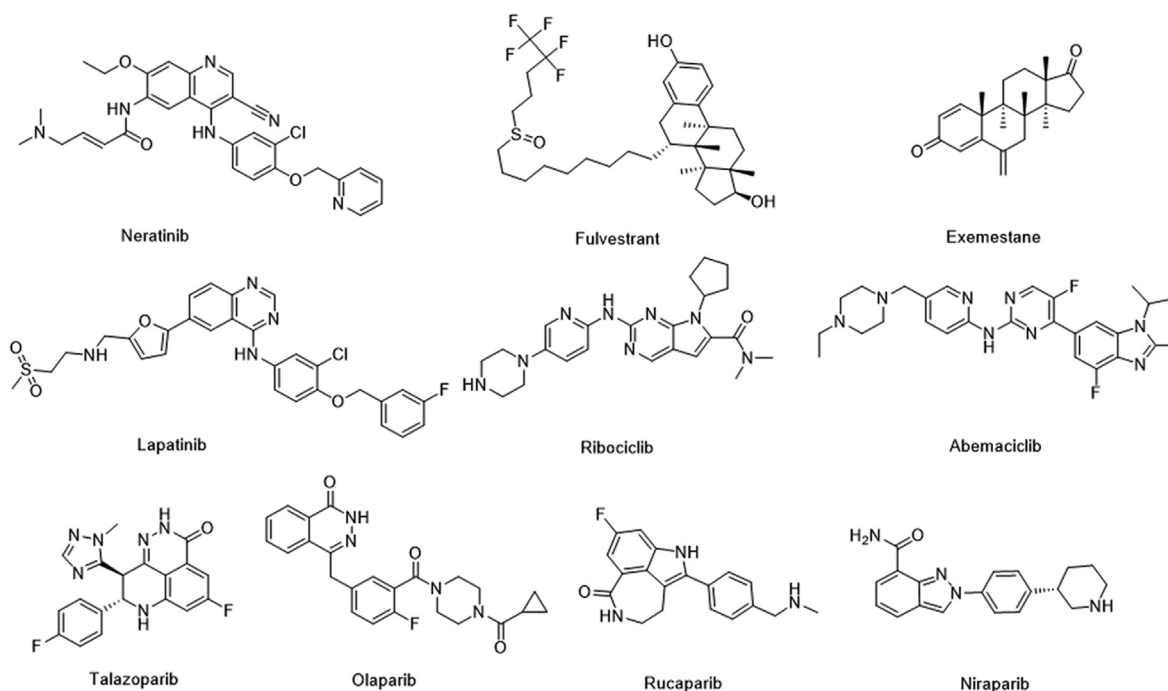


Figure 1 Molecular drugs for breast cancer treatment and four approved PARP-1 inhibitors.

inactivation of either of two genes individually has little effect on cell viability but loss of function of both genes simultaneously leads to cell death^{23,24}. In cancer, the concept of synthetic lethality has been extended to pairs of genes, in which inactivation of one by deletion or mutation and pharmacological inhibition of the other leads to death of cancer cells, whereas normal cells (which lack the fixed genetic alteration) are spared the effect of the drug^{25,26}. Notably, PARP inhibitors based on this concept of synthetic lethality are related to DNA repair pathway and mainly used as drugs in cancer patients with *BRCA1/2* mutations. Mechanically, *BRCA1/2* play an important role in homologous recombination (HR) repair. For some tumor cells, *BRCA1* and *BRCA2* gene mutation, resulting in the cells can not complete DNA repair well. At this time, if a DNA repair inhibitor is applied to tumor cells, it will produce a synthetic lethal effect to kill tumor cells^{27–29}. Although this strategy is very effective, *BRCA1/2* mutations account for only 2%–3% of all breast cancers³⁰. To some extent, this situation limited the wider application of the strategy. Therefore, therapeutic strategies to sensitize *BRCA1/2* wild-type tumors to PARP inhibitors remain to be fully explored^{31,32}. The development of strategies to increase the duration of response of PARP inhibitor and expand the utility of PARP inhibitor to other HR deficient tumors is critical^{33,34}.

Large-scale gene-knockout (using short hairpin RNA (shRNA)-based approaches) studies across many genetic contexts are now being used to map synthetic lethal interactions in human cancer cells^{35,36}. A recent study found that BRD4 shRNA significantly elevated homologous recombination defects (HRD) scores in human THP-1 cells and in murine MLL-AF9/Nras^{G12D} acute myeloid leukemia cells³⁷. In the next in-depth study, the researcher found that BRD4 inhibitors could induce HRD by down regulating the expression of DNA double-strand break (DSB) resection protein C-terminal binding protein interacting protein (CtIP)³⁸. Another study also found that knockdown of BRD4 expression by shRNA to the human, which contributed to decrease the expression of *TOPBP1* and *WEE1*. Both *TOPBP1* and *WEE1* played critical role in DNA replication and DNA damage signaling³⁹. In addition, there were also literature reported that BRD4 mediated the formation of oncogenic gene rearrangements and was critical for nonhomologous end-joining (NHEJ) repair of activation-induced cytidine deaminase and I-SceI-induced DNA breaks^{40,41}. These results indicated that BRD4 played an important role in DNA repair pathway. The bromodomain and extra-terminal domain (BET) protein BRD4 promoted gene transcription by RNA polymerase II, which could mediate signaling transduction to changes in gene regulatory networks⁴². Inhibition of BRD4 may affect DNA repair in more ways^{42,43}. Encouraged by these results, we envisioned that the activity of PARP and BRD4 were inhibited simultaneously to form a synthetic lethal effect and sensitize *BRCA1/2* wild-type cancer cells. Notably, some clinical studies also showed that combination therapy with PARP and BRD4 inhibitor was effective in the treatment of ovarian cancer⁴⁴. Hence, we first identified the possible interaction between PARP and BRD4 in breast cancer by using the system biological network. Considering the advantages of dual-target design drug compared with combination drug^{45–49}, then we rationally designed the first dual-inhibitor of BRD4 and PARP1 by fragment-based combinatorial screening^{50–52}. Through chemical synthesis and structure–activity relationship (SAR) study, the candidate compound **19d**, also named ADTL-BPI1901, was obtained and showed excellent inhibition activities against both targets and favorable *in vivo* antitumor efficacy in *BRCA1/2* wild-

type MDA-MB-468 and MCF-7 xenograft models. The study demonstrated the therapeutic potential of **19d** to target both BRD4 and PARP1, and **19d** may serve as a candidate drug for future breast cancer therapy.

2. Results and discussion

2.1. Bioinformatics analysis

To explore further potential roles of BRD4 and PARP1 in *BRCA* development, protein–protein interaction (PPI) network was established. The BRD4- and PARP1-related proteins were extracted from the total network, and then were further modified by gene ontology and David bioinformatic resources (Fig. 2A). 383 proteins were identified to potentially interact with BRD4 and 1472 proteins were with PARP1 (Fig. 2B). Then, we identified a few of cell cycle and apoptotic hub proteins and relevant signaling pathways that found in the PPI network of BRD4–PARP1 (Fig. 2C).

At last, we evaluated the correlation relation between BRD4 and PARP1 in *BRCA*, and found a significant positive correlation between two targets in *BRCA* from the transcriptome data of breast cancer in the cancer genome atlas (TCGA) database (Fig. 2D). Overall, based on the analysis of existing bioinformatics data, the role of BRD4–PARP1 was associated with cell cycle and apoptosis in breast cancer, which had important cross relation in the global network of breast cancer.

2.2. Fragment-based combinatorial screening to identify lead compound

BRD4 contains two highly conserved N-terminal bromodomains (BD1 and BD2), which have similar sequences. BRD4(BD1) and BRD4(BD2) interact with acetylated chromatin as well as non-histone proteins to regulate transcription, DNA replication, cell cycle progression, and other cellular activities⁵³. In the role of tumor, there have been some reports about the divergent function of BD1 and BD2^{54–56}, but they are still not very clear. Many of the reported BRD4 inhibitors showed highly potent BRD4 inhibitory activity, but due to the high structural homology of acetyl lysine-binding pockets of the BD1 and BD2 domains of BRD4, only a few of them exhibited excellent selectivity for BD1 or BD2 of BRD4^{57,58}. Most of BRD4 inhibitors showed equal affinity for the BD1 and BD2. At present, BRD4 inhibitors can be designed based on two bromine domains BD1 and BD2, respectively. For example, Zhang and Hoelder^{59,60} groups, respectively reported dual inhibitors of BRD4–PLK1 and BRD4–ALK. In their work, they focused on the BD1 domain to design the BRD4 inhibitors. And in another recent study, Liu groups⁶¹ reported that a dual-inhibitors of BRD4–HDAC was designed based on the BD2 domain of BRD4. In this study, we mainly designed BRD4 inhibitors based on BD2 domain.

We firstly summarized the chemical structures of 22 PARP1 inhibitors and 71 BRD4 inhibitors, and split each of them into the core part and fragment part according to their binding modes and structure types (Supporting Information Tables S1 and S2). Subsequently, we constructed the combinatorial compound database in the design and enumerate module of Discovery Studio (version 3.5; San Diego, CA, USA) through three types of connection way: core (BRD4)–core (PARP1), core (BRD4)–fragment (PARP1) and core (PARP1)–fragment (BRD4), and resulted in 1394, 1512,

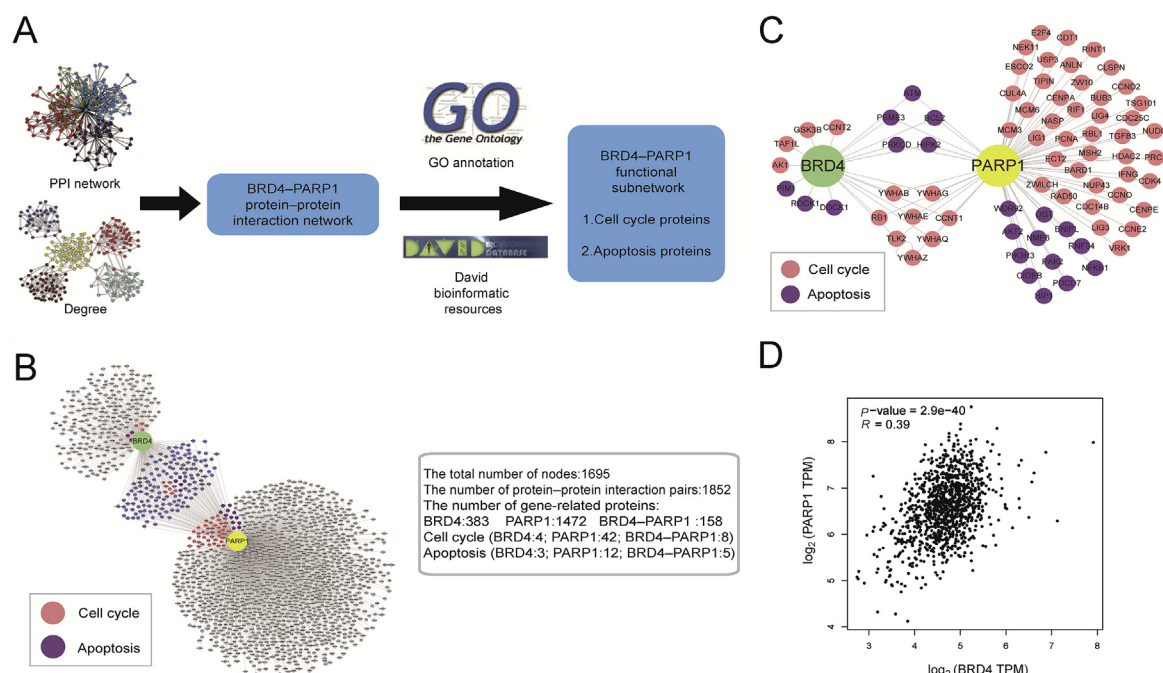


Figure 2 Bioinformatics analysis. (A) Schematic illustration of the workflow of bioinformatics analyses of BRD4–PARP1. (B) Cluster analysis network diagram of BRD4 and PARP1 interaction proteins related to cell cycle, apoptosis. (C) Predicted BRD4- and PARP1-related proteins involved in the regulation of cell cycle and apoptosis, respectively. (D) Correlation between BRD4 and PARP1 in *BRCA*.

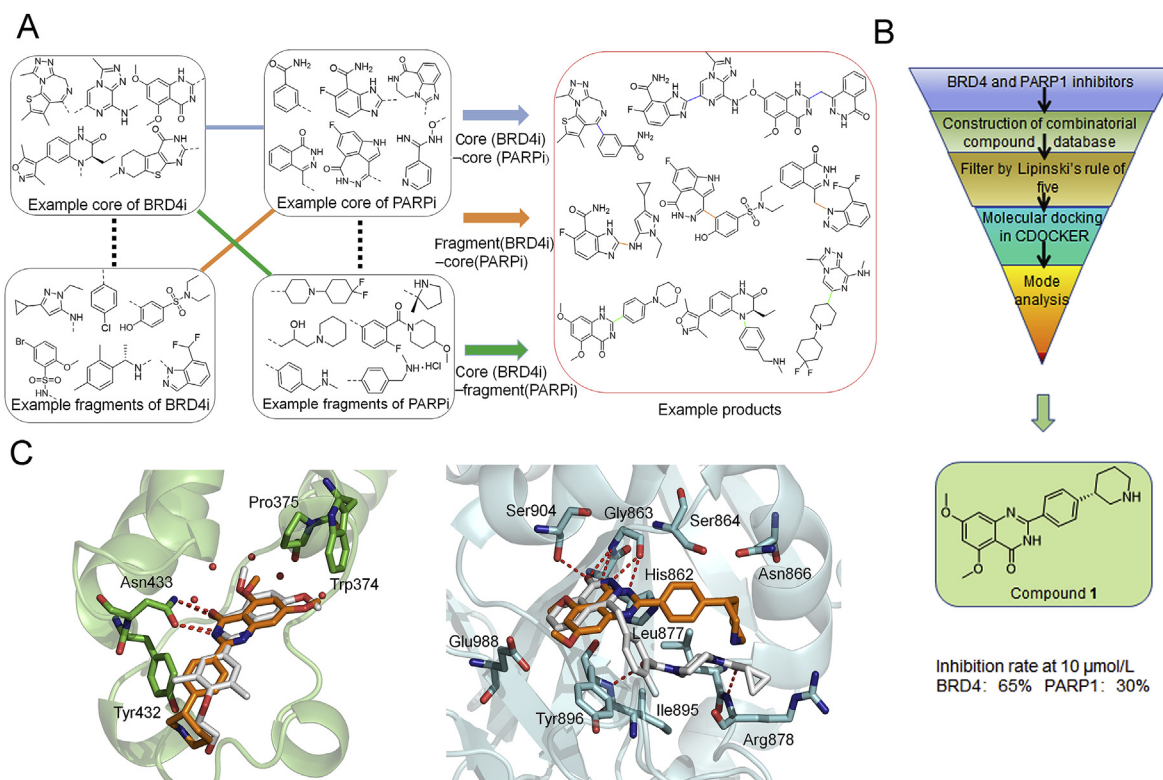


Figure 3 Design strategy of BRD4–PARP1 dual-targeted inhibitor. (A) Design of virtual composite compound library for BRD4 and PARP1. (B) Virtual screening protocol for the identification of the lead compound 1. (C) Predicted binding modes of compound 1 (brown) with BRD4 (green) [PDB ID: 5UOO] and PARP1 (grey) [PDB ID: 5DS3], compared to RVX-208 and Olaparib (white), respectively.

1173 non-redundant compounds, respectively (Fig. 3A). Then, we performed a virtual screening workflow to filter the compound database. The initial combinatorial compound libraries were filtered by the Lipinski's rule of five. The CDOCKER protocol in Discovery Studio was applied to evaluate the binding modes and docking scores between those compounds and the two targets. Finally, based on the ranking of docking scores and the binding mode analysis, comparing to the complex RVX-208–BRD4 and Olaparib–PARP1, 20 potential dual-targeting inhibitors were picked out and tested by experimental assay *in vitro*. As a result, the lead compound **1** (docking score: BRD4 = -7.052 kcal/mol, PARP1 = -6.343 kcal/mol) was determined as the most suitable compound for the ligand binding pocket of BRD4 and PARP1 (Fig. 3B), which could be used for further structural modification.

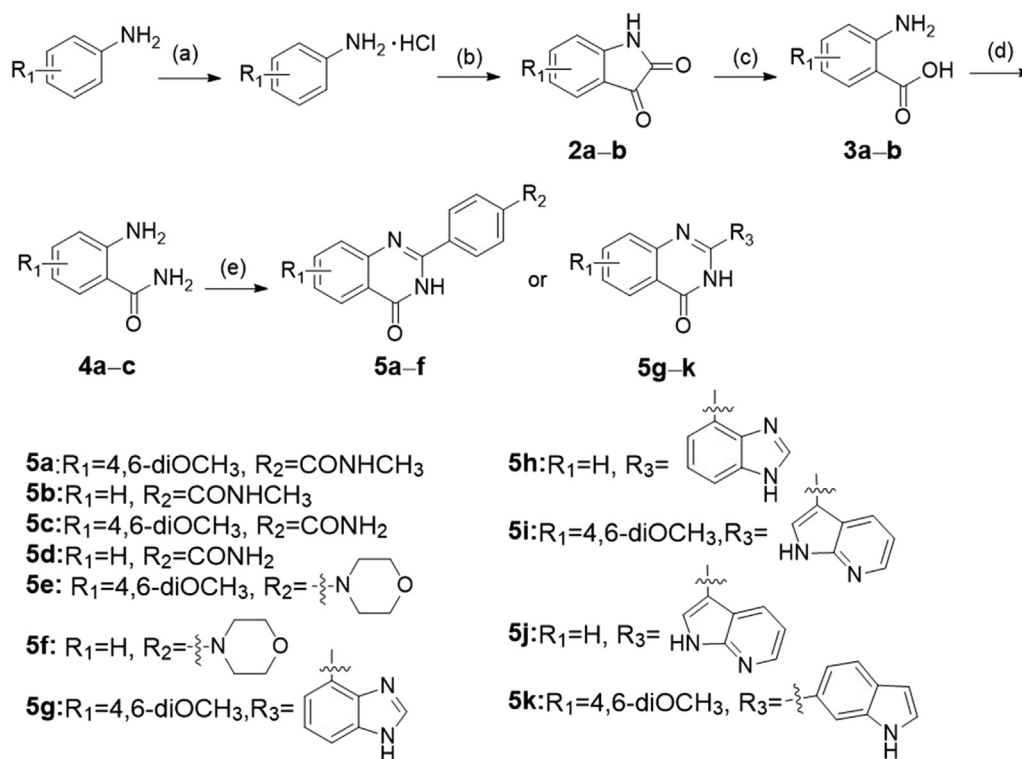
2.3. Synthesis of quinazolin-4(3H)-one derivatives

The synthetic routes of the all target compounds were shown in Schemes 1–4. Compounds **5a–k** were obtained as the procedure described in Scheme 1. Briefly, 3,5-dimethoxyaniline was first converted to the hydrochloride salt, and then the hydrochloride salt was reacted with oxalyl chloride under high temperature. After the simple treatment, the intermediate 4,6-dimethoxyindoline-2,3-dione named **2a** was produced. The ring-opening of **2a** was carried out under strong alkaline conditions, leading to intermediate **3a**. The corresponding **3a** was reacted with concentrated aqueous ammonia to produce key intermediate 2-amino-4,6-dimethoxybenzamide (**4a**) in tetrahydrofuran. The synthesis route of intermediate **4c** (2-amino-6-

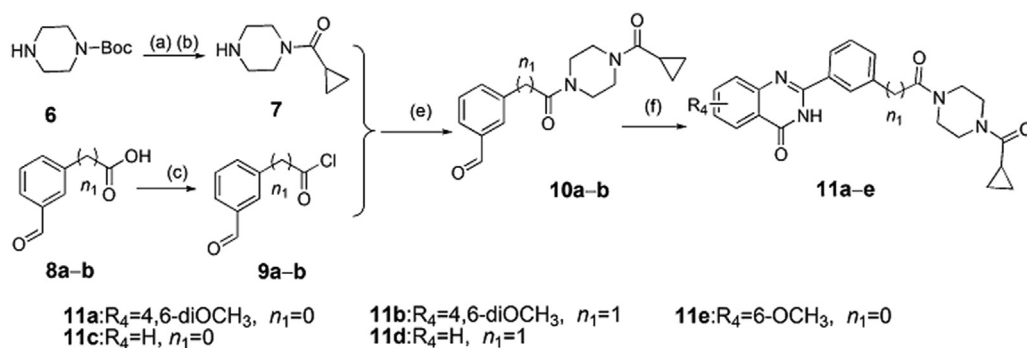
methoxybenzamide) was the same as **4a**. Compound **4b** named 2-aminobenzamide was purchased directly. Finally, intermediates **4a** and **4b** reacted with various aldehydes using *p*-toluenesulfonamide as a catalyst to give target compounds **5a–k** at high temperature for 16–20 h.

The target compounds **11a–e** and **15a–e** were synthesized according to the procedures in Schemes 2 and 3, respectively. In Scheme 2, intermediate **7** was obtained by the reaction of *N*-Boc-piperazine with cyclopropyl acid chloride and *N*-Boc deprotection. Under the condition of heating, the carboxy analogs **8a** and **8b** were treated with thionyl chloride to produce the intermediates **9a** and **9b**. Then, the intermediate **7** reacted, respectively with the intermediates **9a** and **9b** to obtain the compounds **10a** and **10b** by triethylamine in dichloromethane. Finally, target compounds **11a–e** were obtained by the reaction of 2-aminobenzamide analogues (**4a–c**) with intermediates (**10a** and **10b**) at high temperature for 16–20 h. We also synthesized the target compounds **15a–e** in Scheme 3, and the synthetic route was similar with that of in Scheme 2.

The target compounds **19a–v** were synthesized according to the procedure showed in Scheme 4. Commercially available compounds **16a–h** reacted with different dibromoalkanes in *N,N*-dimethylformamide under basic condition of potassium carbonate to produce compounds **17a–h**, which next reacted with different hydroxyl-substituted compounds to give **18a–v** in similar alkaline condition, respectively. Finally, target compounds **19a–v** were obtained in dimethylacetamide by the reaction of 2-amino-4,6-dimethoxybenzamide with **18a–v** at high temperature for 16–20 h, respectively.



Scheme 1 The synthesis of compounds **5a–k**. Reagents and conditions: (a) HCl/Et₂O, overnight, r.t.; (b) (COCl)₂, 160 °C, 2.5 h; (c) NaOH, H₂O₂, 70 °C, 0.8 h; (d) ammonium hydroxide, HOBt, EDCl, NMM, THF, overnight, r.t.; (e) benzaldehyde analogues, DMAC, PTSA, NaHSO₃, 120 °C, 16–20 h.



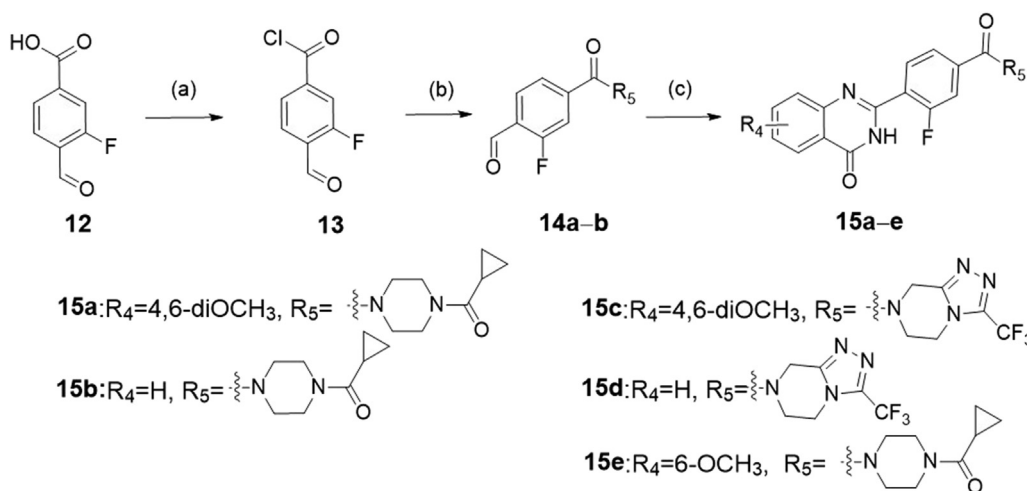
Scheme 2 The synthesis of compounds **11a–e**. Reagents and conditions: (a) cyclopropanecarbonyl chloride, Et_3N , DCM, 0–25 °C, 5 h; (b) HCl/MeOH , 0–25 °C, 4–6 h; (c) thionyl chloride, toluene, 80 °C, 10 h; (e) Et_3N , DCM, 0–20 °C, 3–5 h; (f) 2-aminobenzamide analogues, DMAC, PTSA, NaHSO_3 , 120 °C, 16–20 h.

2.4. Structural optimization of the BRD4 and PARP1 inhibitors

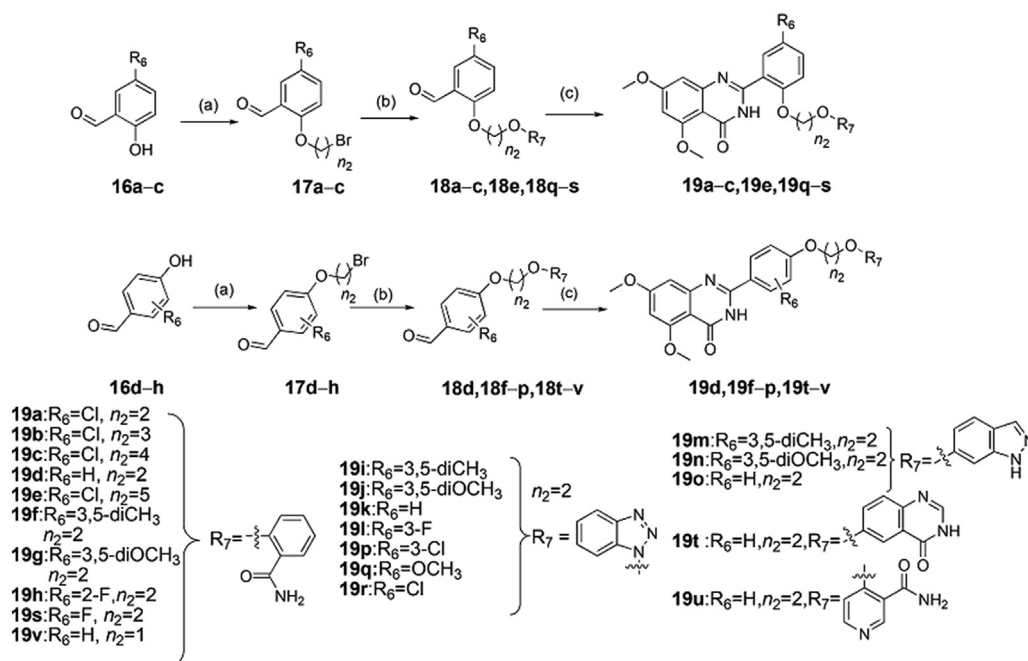
As predicted by docking analysis, compound **1** shared a similar binding mode with typical BRD4 inhibitor RVX-208 and interacted with BRD4 by a linear conformation (Fig. 3C). The carbonyl oxygen and nitrogen atom of the quinazolinone ring system displayed key hydrogen bonding interactions with amide group of Asn433, respectively. The terminal piperidine group was far from Tyr432, which had little effect on the overall activity. For the binding mode of compound **1** with PARP1, similarly, two hydrogen bonds were formed with the backbone atoms of Gly 863, but the terminal group of compound **1** did not completely occupy the entire channel. Moreover, compared to Olaparib, we also found that compound **1** lacked the key hydrogen bond with Ser904 at the core group, and with Arg878 and Tyr896 at the tail group (Fig. 3C). These may be important factors affecting the binding stability and affinities of compound **1** to PARP1. Indeed, lead compound **1** showed a good inhibition rate of BRD4 (up to 65% at 10 $\mu\text{mol/L}$) while the inhibition rate of PARP1 was only 30% at 10 $\mu\text{mol/L}$. Taking into account the presence of large hydrophobic cavity at the PARP1 surface region, the tail group of compound **1** should be further optimized to fit the binding pocket.

The terminal piperidine group was far from Tyr432, which had little overall activity. In this context, we performed the first round of structural optimization by modifying the tail group of compound **1**. The target compounds **5a–k** were first synthesized by introducing substitutions (R_1 and R_2) on the benzene ring and aromatic heterocycle effect on the replacement (R_3). These structures were supposed to form various interactions with the pocket of PARP1. The inhibition rate of compounds **5a–k** for BRD4 and PARP1 were determined at 1 and 10 $\mu\text{mol/L}$ in Table 1, respectively. When R_2 group was morpholine ring, the inhibition rate for BRD4 of compound **5e** could reach to 70%. However, R_3 group was replaced by benzimidazole, indole and azaindole (**5g–k**), the inhibition rates for BRD4 were not further improved. These compounds still had poor inhibitory rate against PARP1 (only up to 39%). Moreover, we found that dimethoxy group might be the key group to inhibit BRD4, and this was similar with RVX-208. We observed that the R_1 group was hydrogen-substituted, the inhibition rates of **5b**, **5d**, **5f**, **5h** and **5j** were relatively low. While the R_1 group was replaced by dimethoxy, the inhibition rates for BRD4 of compounds **5a**, **5e**, **5g** and **5i** were increased.

In order to improve the inhibition rate for PARP1, different moieties contained in reported potent PARP1 inhibitors were



Scheme 3 The synthesis of compounds **15a–e**. Reagents and conditions: (a) thionyl chloride, toluene, 80 °C, 6 h; (b) 1-(cyclopropylcarbonyl) piperazine hydrochloride, or 3-(trifluoromethyl)-5,6,7,8-tetrahydro[1,2,4]triazolo[4,3-*a*]pyrazine, Et_3N , DCM, 0–20 °C, 6–8 h; (c) 2-aminobenzamide analogues, DMAC, PTSA, NaHSO_3 , 120 °C, 16–20 h.



Scheme 4 The synthesis of compounds **19a–v**. Reagents and conditions: (a) various dibromoalkanes, DMF, K₂CO₃, overnight, r.t.; (b) hydroxyl-substituted analogues, DMF, K₂CO₃, r.t., or 80 °C, 8 h; (c) 2-amino-4,6-dimethoxybenzamide, DMAC, PTSA, NaHSO₃, 120 °C, 16–20 h.

analyzed and chosen as the tail group. We found that Olaparib's tail had a bisamide structure, could interact with PARP1's Arg878 and Tyr869 to form two key hydrogen bonds. Thus, we performed the second round of structural optimization by introducing a set of similar structures as substituents attached to the benzene ring. Compounds **11a–e** and **15a–e** were synthesized, and their inhibition rates for BRD4 and PARP1 were tested. When introducing the structure of bisamide on the *meta*-position to the benzene ring, **11** series of compounds exhibited moderate inhibition rates against PARP1 and BRD4 at 10 μmol/L, respectively. When the structure of bisamide was introduced on the *para*-position of the benzene ring, and the fluorine atom was introduced at 2-position simultaneously, the inhibition rates of compound **15a** were increased against PARP1 and BRD4, respectively. Similar trends were observed in the inhibition rates exhibited by other **15** series compounds. Fluorination of pharmaceutical compounds is a common tool to modulate their physicochemical properties⁶². As a consequence of the unique properties of fluorine, fluorine substitution can influence the potency, conformation, metabolism, membrane permeability of a molecule^{63,64}. The fluorine atom at 2-position of the benzene ring may together contribute to the enhancement of the inhibition rate against BRD4 and PARP1. In addition, the inhibition rates of PARP1 could not be significantly increased by extending the structure size of bisamide on the *meta*-position of benzene ring (**Table 2**, **11a** vs. **11c**, **11b** vs. **11d**). Further research found that the substitution of R₄ with hydrogen could obtain better inhibition rate for PARP1 (up to 87% at 10 μmol/L), but the inhibition rate for BRD4 was decreased by 15% (**Table 2**, **15b** vs. **15a**). Binding mode results displayed that the key interaction sites of compound **15b** with PARP1 (Ser904, Gly863 and Arg878) were very similar with Olaparib (Supporting Information **Fig. S2B**). However, compared with RVX-208, there was only one hydrogen bond interaction between **15b** and Cys429 of BRD4. In addition, the conformation of **15b** also dramatically

changed. These results verified again that dimethoxy group was an important group for inhibiting BRD4 activity inhibition. Based on the above analysis, we found that only the tail groups with appropriate size and length could contribute to the improvement of inhibition rate.

In view of the above observations on the SAR, we found that dimethoxy group was favorable to BRD4 inhibition activity, but unfavorable to PARP1 inhibition activity in a certain range of space. In order to find a better balance and produce better inhibitory activity on both BRD4 and PARP1, based on the structure of 5,7-dimethoxy-2-phenylquinazolin-4(3*H*)-one, we further designed other tail structures that can promote the interaction with PARP1. Since the corresponding binding pocket in PARP1 could accommodate flexible linkers with appropriate length, we designed to retain one amide group and use more flexible linker groups to meet the spatial needs. As such, the third round of structural optimization was performed, and compounds **19a–u** were synthesized. The flexible alkyl chain was introduced by oxygen atoms into the *ortho*-position of the benzene ring, and the benzamide group as the monoamide group was attached to the other end of the alkyl chain (**Table 3**, **19a–c** and **19e**). Compound **19a**, with two carbon atoms as the alkyl chain, exhibited good inhibition rate for BRD4 and PARP1 at 10 μmol/L (90% and 85%). However, as the alkyl chain grows, we observed the inhibition rates for PARP1 of the compounds **19b**, **19c** and **19e** were slightly reduced, while the inhibition rates of BRD4 were decreased significantly by up to 36%. Subsequently, we tried to introduce the alkyl chains with two carbon atoms that were introduced onto the *para*-position of the benzene ring (**Table 3**, **19d** and **19f–h**). To our delight, compound **19d** (non-substituents group on the benzene ring vs. **19f–h**) exhibited further enhanced inhibition rate against PARP1 and BRD4 with an inhibition rate of 88% and 92%, respectively. However, for compound **19v**

with shorter alkyl chains ($n_2 = 1$), the inhibition rates against PARP1 and BRD4 were lower than that of **19d**, which were 51% and 60%, respectively. Encouraged by excellent inhibitory activity of **19d**, the more dominant skeletons were introduced to replace benzamide group, which were selected from highly potent PARP1 inhibitors (Table 3, **19i–u**). Unfortunately, no better result had been achieved. In these skeletons, we also investigated the effect of electronegativity of benzene ring on the activity (**19i–u**). The results revealed that regardless of whether the electron-withdrawing group or the electron-donating group was introduced, they all showed poorer activity than non-substituents group on the benzene ring. Through the above repeated and detailed screening, we obtained the optimal compound **19d** toward both targets.

2.5. Inhibitory activities and docking models of compound **19d** with BD1 and BD2 domains of BRD4 and PARP1

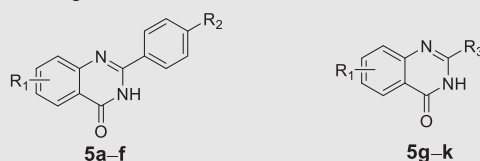
The inhibitory activities of **19d** against BD1 and BD2 domains were tested as shown in Table 4 and Supporting Information Fig. S7. It can be seen that **19d** had IC_{50} of 0.44 $\mu\text{mol/L}$ for BD1 and IC_{50} of 0.379 $\mu\text{mol/L}$ for BD2, which were quite close to the inhibitory activity of BRD4, suggesting that its inhibitory activity against BRD4 may be the comprehensive impact of targeting BD1 and BD2, while targeting BD2 is more important for its subtle selectivity for BD2 against BD1.

Comparing to the inhibitory activities of RVX-208, it indicated that **19d** achieved dual-targeting ability against BRD4 and PARP1 on the loss of its selectivity ability through three rounds of structural optimization. Next, compound **19d** was further assessed in molecular docking to investigate its binding modes with BD1 and BD2 domains of BRD4 and PARP1. As shown in Fig. 4A–D, Supporting Information Fig. S8A–S8D and Table 5, the binding modes of core scaffold of compound **19d** with BD1 and BD2 were quite similar to that of RVX-208. Except for the key hydrogen bonding interactions between quinazolinone ring and amide group of Asn140 in BD1 and Asn433 in BD2, the extended substitution of **19d** with aliphatic chain linking benzamide strengthened the interaction with Asp144 and Asp145 in BD1, and the interaction with Tyr432 and Pro434 in BD2. As for the interaction with PARP1 (Fig. 4E and F, and Supporting Information Fig. S8E and S8F), the binding mode of compound **19d** was also similar to that of Olaparib. **19d** and Olaparib both formed three hydrogen bonds with the hydroxyl group of Ser 904 and the amino group of Gly863, while **19d** formed extra hydrophobic interactions with Ala880, Tyr889, Tyr896 and Ala898 (Table 5).

2.6. SAR summary

Through the three rounds of structural optimization and inhibition rate evaluation for BRD4 and PARP1 of all compounds

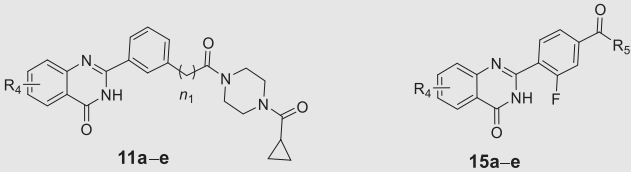
Table 1 Inhibition rates of compounds **5a–k** against PARP1 and BRD4.

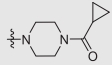
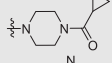
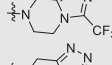
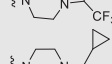
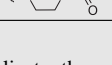


No.	R ₁	R ₂	R ₃	Inhibition rate (1 $\mu\text{mol/L}$ /10 $\mu\text{mol/L}$, %) ^a			
				PARP1 ($\mu\text{mol/L}$)		BRD4 ($\mu\text{mol/L}$)	
				1	10	1	10
5a	4,6-diOCH ₃	CONHCH ₃	—	4	25	1	36
5b	H	CONHCH ₃	—	0	15	0	22
5c	4,6-diOCH ₃	CONH ₂	—	0	2	1	18
5d	H	CONH ₂	—	0	1	2	19
5e	4,6-diOCH ₃		—	2	36	12	70
5f	H		—	0	29	12	55
5g	4,6-diOCH ₃	—		9	34	3	13
5h	H	—		3	10	0	11
5i	4,6-diOCH ₃	—		8	31	7	60
5j	H	—		7	28	6	26
5k	4,6-diOCH ₃	—		6	39	8	42

—Not applicable.

^aEach compound was tested in duplicate, the average value was obtained.

Table 2 Inhibition rates of compounds **11a–e** and **15a–e** against PARP1 and BRD4.


No.	R ₄	R ₅	n ₁	Inhibition rate (1 μmol/L/10 μmol/L, %) ^a			
				PARP1 (μmol/L)		BRD4 (μmol/L)	
				1	10	1	10
11a	4,6-diOCH ₃	—	0	6	57	4	50
11b	H	—	0	16	70	12	43
11c	4,6-diOCH ₃	—	1	8	60	9	47
11d	H	—	1	18	71	4	41
11e	6-OCH ₃	—	0	4	46	8	30
15a	4,6-diOCH ₃		—	14	72	7	68
15b	H		—	6	87	4	53
15c	4,6-diOCH ₃		—	11	55	5	30
15d	H		—	13	60	3	18
15e	6-OCH ₃		—	7	56	9	39

—Not applicable.

^aEach compound was tested in duplicate, the average value was obtained.

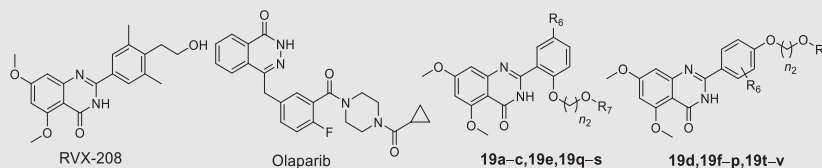
in vitro, the optimal compound **19d** toward two targets was obtained (Fig. 5A and Supporting Information Fig. S2). Meanwhile, as shown in Fig. 5B, the SAR was summarized as follows: (1) the benzamide group of the target compound as an effective group contributes to the inhibitory activity of PARP1 and BRD4; (2) proper linker length is very important. When the length of alkyl chain was two carbon atoms, the target compound possessed the most potent inhibitory activities against BRD4 and PARP1; (3) the dimethoxy group on the quinazolinone is an important group for inhibiting BRD4 activity; (4) different substituents of the R₆ group on the benzene ring had different effects on the inhibitory activity of BRD4 and PARP1, and the hydrogen-substituted target compound had a favorable inhibitory activity against two targets.

2.7. *In vitro* anti-proliferation assay and western blot analysis of compound **19d**

The cell-growth activity of 42 compounds was performed on human breast cancer cell lines MDA-MB-468, MDA-MB-231 and MCF-7 by using MTT assay, respectively. The **19d** exhibited the highest cytotoxic effect in MDA-MB-468 cells and excellent inhibitory activities (Supporting Information Fig. S1 and Table 3). While the synthesis compounds showed weaken anticancer activity in MDA-MB-231 cells. Therefore, we discussed the anti-proliferation activity of **19d** towards MDA-MB-468 and MCF-7

cells (Fig. 6A). For comparison, RVX-208 and Olaparib were used as standard drugs. The activity of **19d** for BRD4 and PARP1 inhibition were summarized in Fig. 6B. The results showed that **19d** exhibited significant inhibitory activities on BRD4 and moderate inhibitory activities on PARP1. As shown in Table 4, compound **19d** exhibited its excellent inhibitory potency against BRD4 with an IC₅₀ of 0.4 μmol/L, improved efficacy > 30-fold than RVX-208 (IC₅₀ = 12.6 μmol/L). But the modest PARP1 inhibitory activity with an IC₅₀ of 4.6 μmol/L was far less than Olaparib (IC₅₀ = 1.3 nmol/L). However, compared with the anti-proliferative activity for MDA-MB-468 cells of Olaparib (IC₅₀ = 1.1 ± 1.4 μmol/L), the compound **19d** showed its parallel anti-proliferative activity toward MDA-MB-468 cells (IC₅₀ = 3.4 ± 1.1 μmol/L). These results may be related to the synthetic lethality. Compound **19d** might play a synthetic lethal role by targeting BRD4 and PARP1 together. Noteworthy, BRD4 regulates HR key effectors, and the present study confirmed that BET inhibition impaired HR-directed double strand breaks repair in *BRCA1/2* wild-type TNBC cells^{65,66}, which might confirm our speculation for these results to some extent. The potential synthetic lethal of compound **19d** suggested that it was functionally inhibiting both BRD4 and PARP1.

Furthermore, Western blot analysis revealed that **19d** showed higher c-Myc inhibition efficiency than RVX-208, and effective downregulation of PAR expression at 2 μmol/L (Fig. 6C and D). Notably, **19d** decreased the expression of c-Myc and PAR in a

Table 3 Inhibition rates and *in vitro* anti-proliferative activity of compounds **19a–v**.

No.	R ₆	R ₇	n ₂	Inhibition rate (1 μmol/L/10 μmol/L, %) ^a				Anti-proliferative activity (IC ₅₀ , μmol/L) ^b
				PARP1 (μmol/L)		BRD4 (μmol/L)		
				1	10	1	10	
RVX-208	—	—	—	1	4	20	60	>30
Olaparib	—	—	—	100	100	—	—	1.1 ± 1.4
19a	Cl		2	30	85	31	90	6.0 ± 0.9
19b	Cl		3	35	81	3	69	10.9 ± 0.5
19c	Cl		4	29	84	7	54	7.4 ± 1.8
19d	H		2	37	88	69	92	3.4 ± 1.1
19e	Cl		5	18	71	4	55	15.3 ± 3.6
19f	3,5-diCH ₃		2	40	79	11	74	8.4 ± 1.3
19g	3,5-diOCH ₃		2	25	70	15	72	5.7 ± 2.1
19h	2-F		2	31	65	12	62	11.8 ± 3.4
19i	3,5-diCH ₃		2	11	18	18	61	>30
19j	3,5-diOCH ₃		2	6	18	12	64	>30
19k	H		2	7	29	13	83	22.9 ± 2.4
19l	3-F		2	1	14	29	80	23.7 ± 3.3
19m	3,5-diCH ₃		2	7	11	15	46	>30
19n	3,5-diOCH ₃		2	9	16	14	45	>30
19o	H		2	3	13	3	56	>30
19p	3-Cl		2	3	6	3	44	>30
19q	OCH ₃		2	3	2	11	80	24.2 ± 2.2
19r	Cl		2	4	6	17	77	>30
19s	F		2	12	65	8	74	8.7 ± 5.2
19t	H		2	1	25	9	67	>30
19u	H		2	36	81	6	77	6.7 ± 2.4
19v	H		1	19	51	29	60	—

—Not applicable or not test.

^aEach compound was tested in duplicate, the average value was obtained.^bIC₅₀ values were obtained with cell viability assay for 24 h.

Table 4 IC₅₀ of **19d** against BRD4 and PARP1 compared with RVX-208 and Olaparib.

Molecular	IC ₅₀ (μmol/L)			
	BRD4	PARP1	BRD4(BD1)	BRD4(BD2)
Rvx-208	12.7	—	1.387	0.053
Olaparib	—	0.0013	—	—
19d	0.4	4.6	0.44	0.379

—Not applicable.

dose-dependent manner (Fig. 6E). Consistent with our design strategy, these data showed that **19d** was indeed an effective BRD4 and PARP1 dual inhibitor.

2.8. Cell cycle analysis and apoptosis assays

BRD4 and PARP1 were two regulators of cell proliferation by positive affect the cell cycle. To clarify the mechanism of the anti-

proliferation effect of **19d**, we firstly employed the cell cycle analysis. The MDA-MB-468 cells and MCF-7 cells were treated with different concentration of **19d**. The percentage of cells in the G1, S, and G2/M phases was significantly changed in MDA-MB-468 cells. The percentage of MDA-MB-468 cells in G1 was remarkably increased and the percentage in G2/M phase significantly declined in a dose-dependent manner (Fig. 7A). However, there were no significant changes in 1 μmol/L **19d** treatment during the G1 and G2/M phases compared to 3.3 and 10 μmol/L **19d** treated MCF-7 cells (Supporting Information Fig. S6A). The results confirmed that the **19d** interfered the cell cycle at the G1 phase, especially in MDA-MB-468 cells. Subsequently, we detected whether **19d** could induce apoptosis. The results suggested that **19d** induced apoptosis in a dose-dependent manner (Fig. 7B). There were no significant changes in **19d** treated MCF-7 cells (Supporting Information Fig. S6B). Next, Western blot analysis revealed that BCL-2 expression was remarkably down-regulated, but BAX and the active form of caspase-3 expression were increased after **19d** treatment (Fig. 7C). In the colony

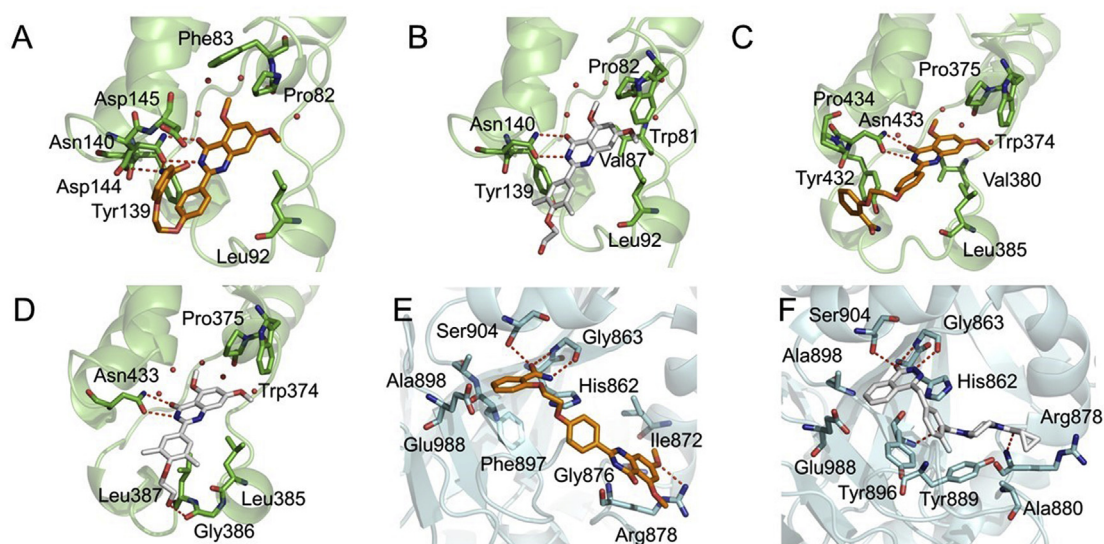


Figure 4 Binding mode analysis of **19d**, RVX-208 and Olaparib. (A) and (B) Binding mode of **19d** and RVX-208 in the BD1 domain of BRD4. BRD4 (PDB code: 4MR4) was shown in green. (C) and (D) Binding mode of **19d** and RVX-208 in the BD2 domain of BRD4. BRD4 (PDB code: 5UOO) was shown in green. (E) and (F) Binding mode of **19d** and Olaparib in the active site of PARP1. PARP1 (PDB code: 5DS3) was shown in cyan. The carbon atoms of **19d** were colored in orange, while RVX-208 and Olaparib were colored in white. The oxygen atoms were colored in red and nitrogen atoms in blue. Hydrogen bonds were indicated with dashed lines.

Table 5 Comparison of key residues of **19d**, RVX-208, Olaparib in protein BRD4 and PARP1 binding patterns.

Molecular	Docking score (kcal/mol)			Interactive residues (within 2.5 Å)		
	BRD4(BD1)	BRD4(BD2)	PARP1	BRD4(BD1)	BRD4(BD2)	PARP1
Rvx-208	-6.96	-7.60	—	Trp81, Pro82, Val87, Leu92, Tyr139, Asn140	Trp374, Pro375, Leu385, Gly386, Leu387, Asn433	—
Olaparib	—	—	-10.94	—	—	His862, Gly863, Arg878, Ala880, Tyr889, Tyr896, Ala898, Ser904, Glu988
19d	-8.80	-7.23	-7.51	Pro82, Phe83, Leu92, Tyr139, Asn140, Asp144, Asp145	Trp374, Pro375, Tyr432, Asn433, His437, Glu438	His862, Gly863, Arg878, Ala898, Ile872, Gly876, Phe897, Ser904, Glu988

—Not applicable.

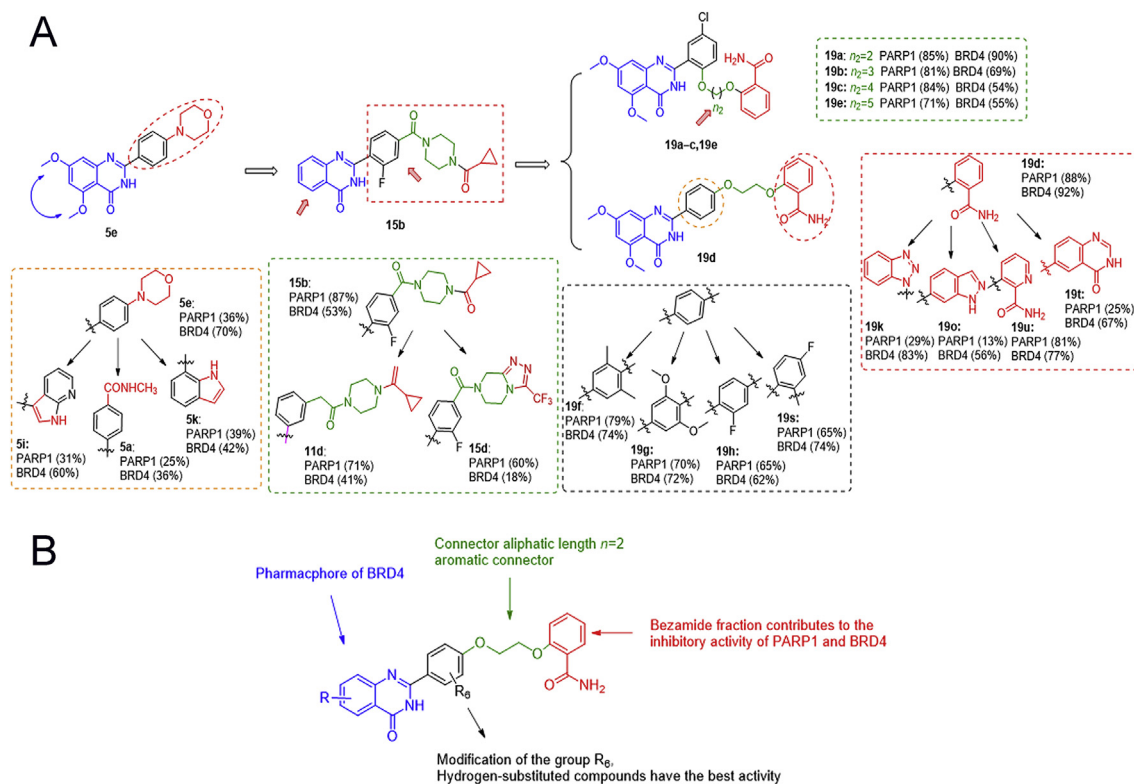


Figure 5 Structural optimization and discovery of the dual target inhibitors. (A) Target inhibitory activities evaluation *in vitro* guided optimization toward **19d**. (B) SAR summary of BRD4 and PARP1 dual inhibitors.

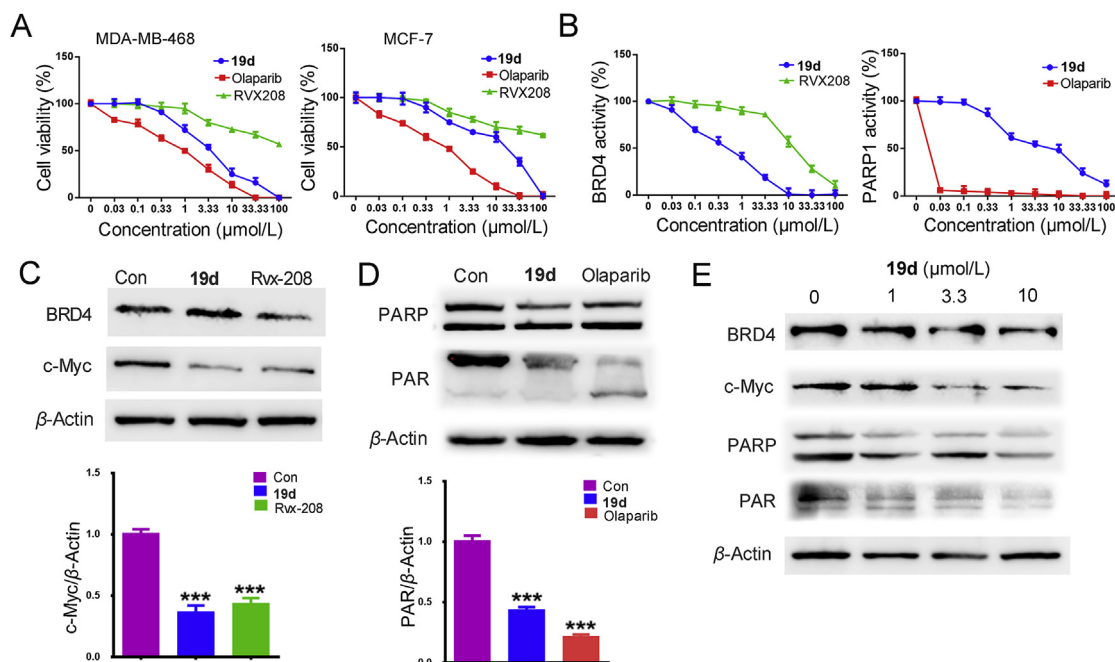


Figure 6 Identification of candidate compound **19d**. (A) The anti-proliferation activity of **19d**, RVX-208 and Olaparib towards MDA-MB-468 and MCF-7 cells. (B) The inhibitory activity of **19d**, RVX-208 and Olaparib for BRD4 and PARP1 were detected by activity assay in diverse concentrations. (C) MDA-MB-468 cells treated with **19d** and RVX-208 for 24 h at 2 $\mu\text{mol/L}$, the expression of BRD4 and c-Myc were detected by Western blot. β -Actin was used as a loading control. (D) MDA-MB-468 cells treated with **19d** and Olaparib for 24 h at 2 $\mu\text{mol/L}$, the expression of PARP and PAR were detected by Western blot. β -Actin was used as a loading control. (E) MDA-MB-468 cells treated with DMSO, 1, 3.3 and 10 $\mu\text{mol/L}$ of **19d** for 24 h, the expression levels of BRD4, c-Myc, PARP and PAR were detected by Western blot. β -Actin was used as a loading control. *** $P < 0.001$ compared with control group. Data are present as means \pm SD, $n = 3$.

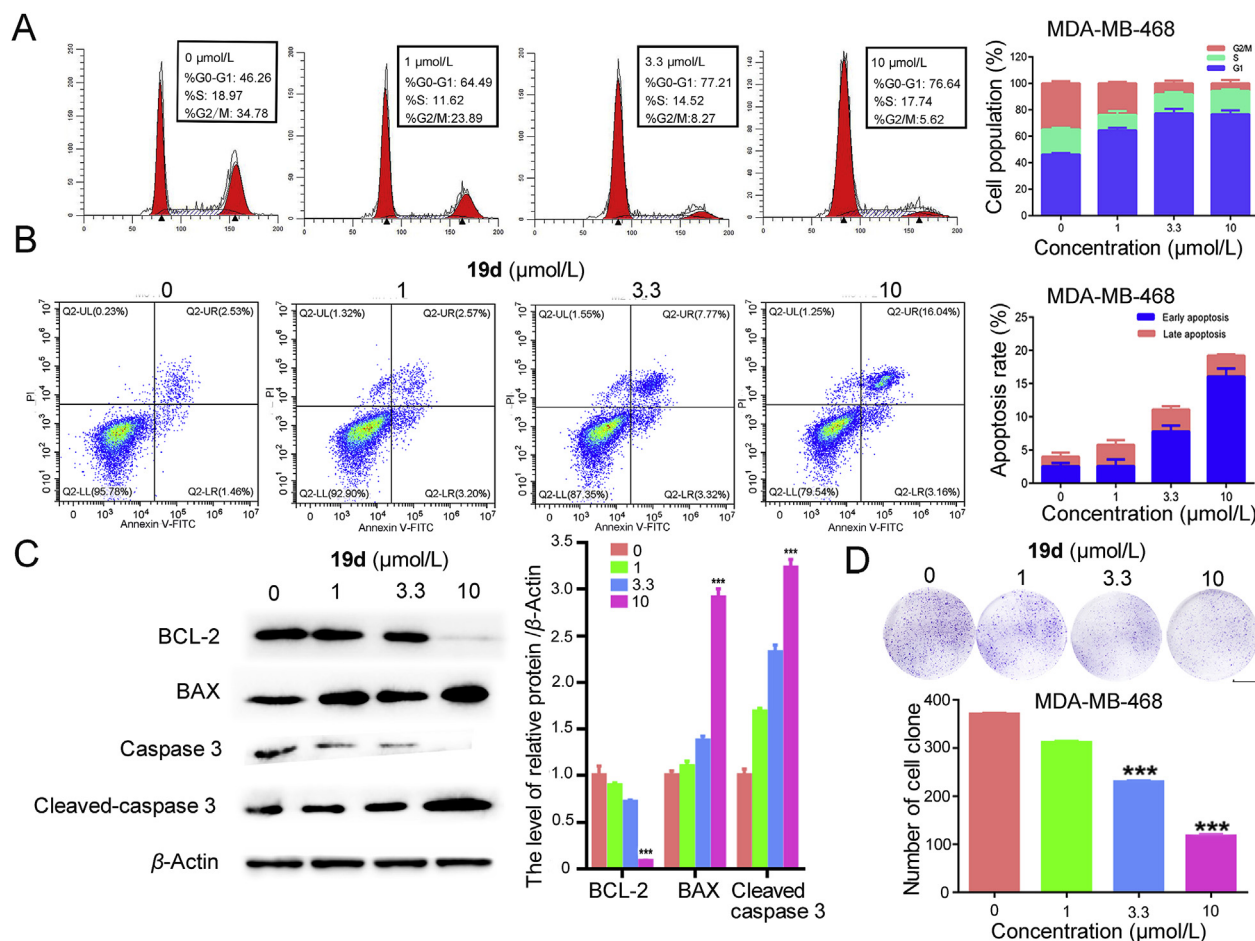


Figure 7 The mechanism of **19d**-induced MDA-MB-468 cells death. (A) Cell cycle distribution of MDA-MB-468 cells was measured by flow cytometry using propidium iodide (PI) staining. (B) Apoptosis rates of MDA-MB-468 cells were detected by Annexin V-fluorescein isothiocyanate isomer I (FITC)/PI staining after treatment with **19d**. (C) After DMSO, 1, 3.3 and 10 μmol/L of **19d** treatment in MDA-MB-468 cells, the expression levels of BCL-2, BAX and caspase 3 were determined by Western blot analysis. β-Actin was measured as loading control. (D) Colony formation assay was used to detect the proliferation ability in MDA-MB-468 cells after treatment of compound **19d**. Scale bar: 10 mm. The statistics of the colony counts. *** $P < 0.001$ compared with control group. Data are present as means \pm SD, $n = 3$.

formation assay, compound **19d** remarkably decreased the colony counts compared with the DMSO-treated control group (Fig. 7D). Taken together, these results indicated that **19d** interfered the cell cycle arrest at G1 phase, suppressed cloning formation, and promoted apoptosis in MDA-MB-468 cells. However, it only showed slight activity on MCF-7 cells (Supporting Information Fig. S6). These results indicated that **19d** was more effective on triple negative breast cancer.

2.9. Pharmacokinetics (PK) profiles of compound **19d**

Based on its closely matched BRD4/PARP1 inhibitory activity, potent anti-proliferative and proapoptotic capacities, compound **19d** was progressed into an *in vivo* pharmacokinetic study. As shown in Table 6, plasma PK after 10 mg/kg oral administration of compound **19d** to Sprague–Dawley (SD) rats was characterized. Compound **19d** showed a good elimination half-life ($t_{1/2}$) of 3.1 h with an $AUC_{0-\infty}$ of 144.7 h·ng/mL. The oral maximum plasma concentration (C_{max}) was 26.65 ng/mL, T_{max} was 1.58 h, and the mean residence time (MRT) was 5.35 h. These favorable pharmacokinetic properties of compound **19d** apprehended its suitability for using as oral candidate.

2.10. *In vivo* xenograft model experiments of compound **19d**

Encouraged by the excellent potency *in vitro* as well as the acceptable PK profiles, **19d** was further progressed into *in vivo* antitumor activity studies. In the MDA-MB-468 breast cancer xenograft model, oral doses of mice with 20, 40 and 80 mg/kg of **19d** were chose based on the preliminary experiment and other

Table 6 PK profiles of compound **19d** in SD rats ($n = 3$).

Parameter	Rat ^a <i>p.o.</i> (10 mg/kg)
$t_{1/2}$ (h)	3.10 \pm 0.12
T_{max} (h)	1.58 \pm 0.35
$MRT_{0-\infty}$ (h)	5.35 \pm 0.44
C_{max} (ng/mL)	26.65 \pm 3.66
AUC_{0-t} (h·ng/mL)	114.43 \pm 15.81
$AUC_{0-\infty}$ (h·ng/mL)	144.72 \pm 25.51

^aData are present as means \pm SD, $n = 3$.

previous studies^{67–70}, which achieved a dose-dependent tumor growth inhibition (TGI) effect. Medium dose and high dose groups showed similar inhibitory effects, with a TGI of 55.3% for 80 mg/kg. In this model, slight body weight change and no death of mice were observed during the treatment period. These results indicated that **19d** exhibited potent antitumor effect without significant toxicity (Fig. 8A). To deep validate its dual antitumor mechanism, immunohistochemistry (IHC) staining was performed and showed that the expression levels of BRD4 and PARP1 were effectively suppressed in tumor tissues of the **19d** 40 mg/kg treatment groups compared with the control group (Fig. 8C).

Further, the inhibition effect in MCF-7 breast cancer xenograft model was also evaluated. As shown, a similar TGI rate of 48.3% was observed in 80 mg/kg treatment group, and with slightly body weight increase in all the groups, indicating no apparent toxicity of all the dosages used here (Fig. 8B). In the IHC staining assay, the expression levels of BRD4 and PARP1 were slightly down-regulated in the tumor tissues of the **19d** treatment groups (Supporting Information Fig. S3). In addition, hematoxylin-eosin (HE) histology study in the major organs (heart, lung, liver, spleen, and kidney) of all the groups was conducted after **19d** treatment (Supporting Information Figs. S4 and S5), and **19d** showed no visible histological changed, indicating no apparent toxicity of **19d**.

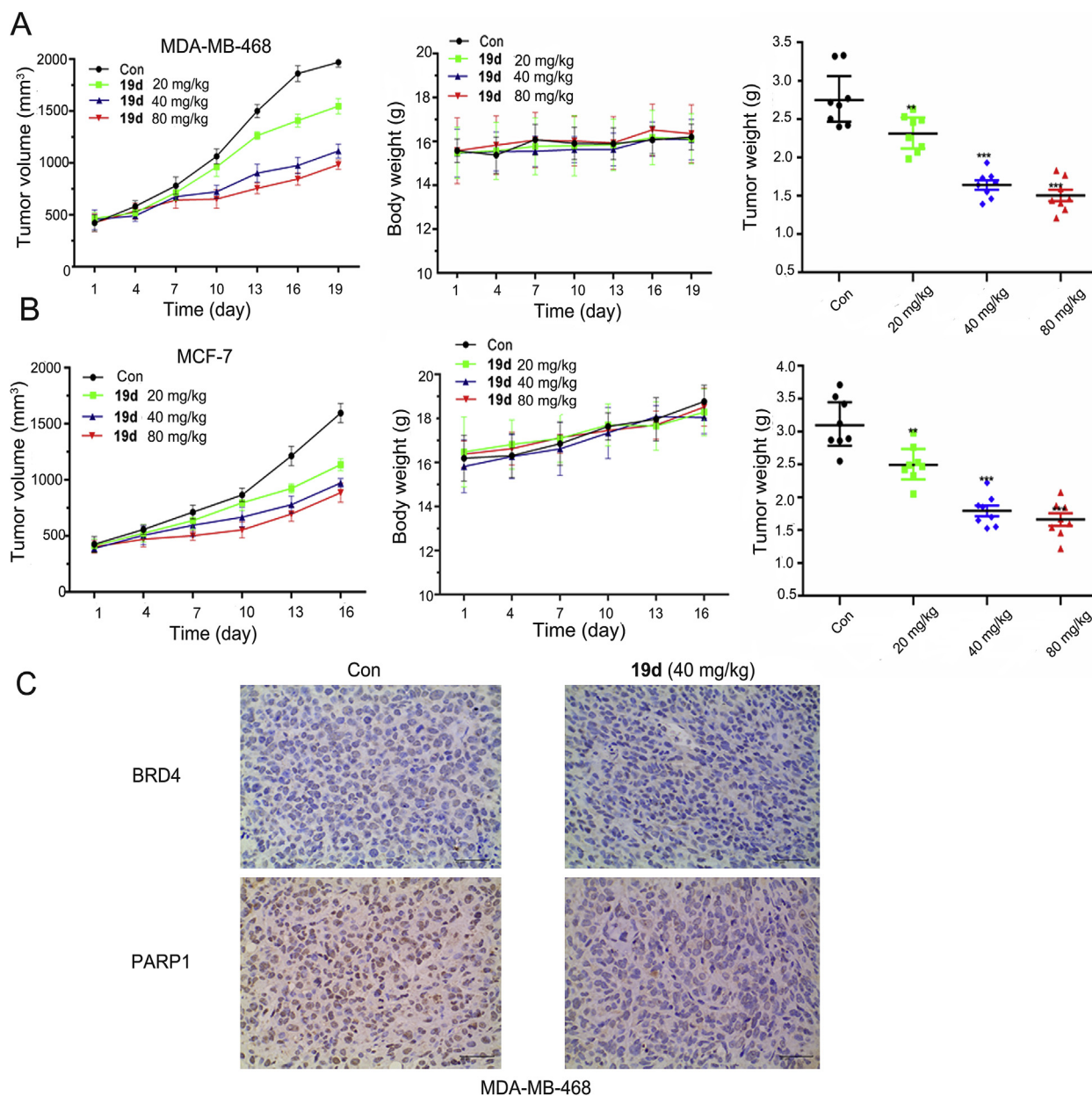


Figure 8 *In vivo* antitumor efficacy of compound **19d** in the MDA-MB-468 tumor xenograft model and the MCF-7 tumor xenograft model. (A) Tumor volume changes, average body weights and tumor weights following the treatment of **19d** at oral doses of 20, 40 and 80 mg/kg in the MDA-MB-468 tumor xenograft model. (B) Tumor volume changes, average body weight and tumor weight following the treatment of **19d** at oral doses of 20, 40 and 80 mg/kg in the MCF-7 tumor xenograft model. (C) Immunohistochemical staining of PARP1 and BRD4 in the MDA-MB-468 tumor tissues from 40 mg/kg of **19d**-treated mice and vehicle groups (200 ×), respectively.

3. Conclusions

In summary, as a result of cross roles between BRD4 and PARP1 of the synthetic lethality mechanism, the important relation of them was further identified through the global PPI network in breast cancer. Therefore, we performed a virtual screening workflow to filter the compounds and got the lead compound **1** based on reported BRD4 and PARP1 inhibitors, the optimal compound **19d** (named ADTL-BPI901) was obtained and both exhibited potential enzymatic potencies against BRD4 and PARP1 through the three rounds of structural optimization. Further experiments demonstrated that **19d** efficiently modulated the expression of BRD4 and PARP1. Compound **19d** could induce breast cancer cell apoptosis and stimulated cell cycle arrests at G1 phase. Following PK studies, **19d** showed its excellent antitumor activity in *BRCA1/2* wild-type MDA-MB-468 and MCF-7 xenograft models without causing remarkable loss of body weight and toxicity. Overall, the superior inhibition effect of compound **19d** was systematically investigated and validated *via in vitro* and *in vivo* experiments. As the first potent dual-target inhibitor of BRD4 and PARP1 based on the concept of synthetic lethality, which shows favorable safety profiles that represents a promising candidate small-molecule drug for the future treatment of breast cancer.

4. Experimental

4.1. General methods of chemistry

All anhydrous solvents and reagents were obtained from commercial sources and used without further purification. Evaporation of solvent was carried out by using a rotary evaporator (N-1100, Eyela, Tokyo, Japan) under reduced pressure. ^1H NMR and ^{13}C NMR spectra were recorded at 400 and 100 MHz by nuclear magnetic resonance spectroscopy (BrukerAV III-400, Karlsruhe, Germany), respectively. The chemical shifts were reported by using TMS as an internal standard and CDCl_3 or $\text{DMSO}-d_6$ as solvents. The isolation of compounds was carried out on silica gel (300–400 mesh, Qingdao Marine Chemical Ltd., Qingdao, China). The progress of the reaction was detected by thin-layer chromatography (TLC) using silica gel plates (silica gel 60 F254, Qingdao Marine Chemical Ltd, Qingdao, China). High-resolution mass spectra (ESI-HR-MS) data were recorded on a commercial apparatus, and methanol was used to dissolve the sample. High-performance liquid chromatography (HPLC) was performed by Wates e2695 (Shanghai, China) with Thermo C18-WR column (5.0 μm , 250 mm \times 4.6 mm). HPLC conditions: liquid phase MeOH/ H_2O at a flow rate of 1.0 mL/min. All chemical structures were performed by ChemBioDraw software (version 14.0).

4.2. General synthetic information of target compounds

4.2.1. Preparation of compound **2a**: 4,6-dimethoxyindoline-2,3-dione

3,5-Dimethoxyaniline (6.0 g, 38.2 mmol) was dissolved in ether (80 mL) and stirred at 0 °C. Saturated hydrochloric acid/ether solutions (15 mL) was bubbled into the reaction mixture for 20 min. The reaction mixture was removed to room temperature for 4 h and then filtered; the residue was washed with cooled ethyl acetate and dried *in vacuo* to give the corresponding hydrochloride salt (8 g, 98%). The hydrochloride salt of aniline **1** (3.5 g,

18.45 mmol) was dissolved in oxalyl chloride (5.3 mL), and the reaction mixture was heated to 170 °C for 2.5 h. The solvent was removed under reduced pressure. The reaction mixture was diluted with MeOH (15 mL) at 0 °C and then heated to reflux for 1 h. The reaction mixture was hot filtered, and the precipitate was washed with MeOH to give compound **2a** (2.9 g, 52%–69% yield) which was used without further purification. ^1H NMR (400 MHz, $\text{DMSO}-d_6$), δ (ppm): 10.92 (1H, brs), 6.17 (1H, d, $J = 1.9$ Hz), 6.02 (1H, d, $J = 1.9$ Hz), 3.88 (3H, s), 3.87 (3H, s).

4.2.2. Preparation of compound **3a**: 2-amino-4,6-dimethoxybenzoic acid

A solution of compound **2a** in NaOH (33% in water, 19 mL) was heated to 70 °C. H_2O_2 (30% in water, 4.7 mL) was added to the solution dropwise. The mixture was maintained at 70 °C for 50 min. Saturated $\text{Na}_2\text{S}_2\text{O}_3$ solution (18 mL) was added to the above mixture at 10 °C. The reaction mixture was adjusted to pH = 8 with HCl and then to pH = 5 with acetic acid. The precipitate that formed was collected, washed with water, and dried to give the title compound **3a** (1.2 g, 24%–33% yield). ^1H NMR (400 MHz, CDCl_3), δ (ppm): 11.05 (1H, s), 6.43 (2H, s), 5.82 (2H, s), 3.95 (3H, s), 3.78 (3H, s).

4.2.3. Preparation of compound **4a**: 2-amino-4,6-dimethoxybenzamide

A mixture of EDCI (0.75 g, 3.8 mmol), HOBT (0.50 g, 3.8 mmol), and NMM (0.38 g, 3.8 mmol) were added to a solution of 2-amino-4,6-dimethoxybenzoic acid (0.50 g, 2.55 mmol) in THF (15 mL). The mixture was stirred for 10 min, and then ammonium hydroxide (50% *v/v* aqueous solution) was bubbled through at room temperature, stirred overnight. Water was added (5 mL), and the aqueous layer was extracted with DCM (3 \times 25 mL). The organic layers were combined, washed with water (3 \times 25 mL), dried (Na_2SO_4), and concentrated *in vacuo*. The residue was purified by flash column chromatography (DCM/MeOH = 80:1) to give the title compound **4a** (0.43 g, 84% yield). ^1H NMR (400 MHz, $\text{DMSO}-d_6$), δ (ppm): 7.45 (1H, s), 7.01 (1H, s), 6.89 (2H, s), 5.88 (1H, d, $J = 2.4$ Hz), 5.76 (1H, d, $J = 2.4$ Hz), 3.76 (3H, s), 3.68 (3H, s). The synthetic route of compound **4c** named 2-amino-6-methoxybenzamide was the same as that of compound **4a**.

4.2.4. Preparation of target compounds **5a–f** and **5g–k**

2-Aminobenzamide analogues (**4a** and **4b**, 0.86 mmol, 1 equiv.) and benzaldehyde analogues (0.86 mmol, 1 equiv.) were dissolved in DMAc (12 mL) and treated with sodium hydrogen sulfite (1.03 mmol, 1.2 equiv.) and PTSA (0.21 mmol, 0.24 equiv.). The reaction mixture was stirred at 120 °C for 16–20 h. Water (80 mL) was added to the reaction, and the precipitated solid was collected by filtration. Purification of this solid by silica gel chromatography (dichloromethane/methanol = 40:1–20:1) gave final compounds **5a–k** (37%–61% yield).

4.2.4.1. 4-(5,7-Dimethoxy-4-oxo-3,4-dihydroquinazolin-2-yl)-*N*-methylbenzamide (**5a**). Light yellow solid, Yield 56%. m.p. 221–224 °C. ^1H NMR (400 MHz, $\text{DMSO}-d_6$), δ (ppm): 11.56 (1H, brs), 10.20 (1H, s), 8.13 (2H, d, $J = 8.7$ Hz), 7.71 (2H, d, $J = 8.7$ Hz), 6.75 (1H, d, $J = 2.2$ Hz), 6.54 (1H, d, $J = 2.2$ Hz), 3.89 (3H, s), 3.85 (3H, s), 2.09 (3H, s). ^{13}C NMR (100 MHz, $\text{DMSO}-d_6$), δ (ppm): 169.2, 164.7, 161.4, 160.2, 153.6, 152.8, 142.6, 128.9, 126.9, 118.8, 105.1, 101.6, 97.9, 56.4, 56.0, 24.6.

HR-MS (ESI) Calcd. for $C_{18}H_{18}N_3O_4$ $[M+H]^+$: m/z 340.1297, Found 340.1294.

4.2.4.2. *N-Methyl-4-(4-oxo-3,4-dihydroquinazolin-2-yl)benzamide (5b)*. Off-white solid, Yield 48%. m.p. 233–235 °C. 1H NMR (400 MHz, DMSO- d_6), δ (ppm): 12.39 (1H, brs), 10.22 (1H, s), 8.17–8.13 (3H, m), 7.84–7.80 (1H, m), 7.75–7.70 (3H, m), 7.51–7.47 (1H, dd, $J = 7.4$ Hz, 7.2 Hz), 2.09 (3H, s). ^{13}C NMR (100 MHz, DMSO- d_6), δ (ppm): 169.2, 162.7, 152.3, 149.3, 142.6, 135.0, 128.9, 128.9, 127.8, 127.2, 126.7, 126.3, 121.2, 118.8, 118.7, 24.8. HR-MS (ESI) Calcd. for $C_{16}H_{14}N_3O_2$ $[M+H]^+$: m/z 280.1086, Found 280.1088.

4.2.4.3. *4-(5,7-Dimethoxy-4-oxo-3,4-dihydroquinazolin-2-yl)benzamide (5c)*. Light yellow solid, Yield 56%. m.p. 201–203 °C. 1H NMR (400 MHz, DMSO- d_6), δ (ppm): 12.11 (1H, brs), 8.23 (2H, d, $J = 8.3$ Hz), 8.00 (2H, d, $J = 8.3$ Hz), 6.78 (1H, d, $J = 2.2$ Hz), 6.56 (1H, d, $J = 2.2$ Hz), 3.90 (3H, s), 3.86 (3H, s). ^{13}C NMR (100 MHz, DMSO- d_6), δ (ppm): 164.8, 164.7, 161.5 (2C), 159.2, 153.4, 152.1, 143.7, 123.5, 122.2, 105.4, 102.0, 101.9, 98.2 (2C), 56.48, 56.15. HR-MS (ESI) Calcd. for $C_{17}H_{16}N_3O_4$ $[M+H]^+$: m/z 326.1141, Found 326.1137.

4.2.4.4. *4-(4-Oxo-3,4-dihydroquinazolin-2-yl)benzamide (5d)*. Off-white solid, Yield 49%. m.p. 235–237 °C. 1H NMR (400 MHz, DMSO- d_6), δ (ppm): 12.61 (1H, brs), 8.27 (2H, d, $J = 8.5$ Hz), 8.18 (1H, d, $J = 7.2$ Hz), 8.04 (2H, d, $J = 8.5$ Hz), 7.88–7.84 (1H, m), 7.57–7.53 (2H, m). ^{13}C NMR (100 MHz, DMSO- d_6), δ (ppm): 167.6, 162.6, 152.1, 149.0, 137.0, 135.5, 135.1, 128.2, 128.1 (3C), 128.0, 127.3, 126.3, 121.6. HR-MS (ESI) Calcd. for $C_{15}H_{12}N_3O_2$ $[M+H]^+$: m/z 266.0930, Found 266.0933.

4.2.4.5. *5,7-Dimethoxy-2-(4-morpholinophenyl)quinazolin-4(3H)-one (5e)*. Off-white solid, Yield 43%. m.p. 188–190 °C. 1H NMR (400 MHz, $CDCl_3$), δ (ppm): 9.46 (1H, brs), 7.93 (2H, d, $J = 8.8$ Hz), 6.78 (1H, d, $J = 2.1$ Hz), 6.62 (2H, d, $J = 8.8$ Hz), 6.38 (1H, d, $J = 2.1$ Hz), 3.97 (3H, s), 3.92 (3H, s), 3.39–3.36 (4H, m), 2.07–2.03 (4H, m). ^{13}C NMR (100 MHz, DMSO- d_6), δ (ppm): 164.6 (2C), 161.4 (2C), 160.4, 153.4, 150.2, 129.4 (2C), 111.5 (2C), 104.6, 100.9, 97.2, 56.3, 56.0, 47.7 (2C), 25.4 (2C). HR-MS (ESI) Calcd. for $C_{20}H_{22}N_3O_4$ $[M+H]^+$: m/z 368.1610, Found 368.1608.

4.2.4.6. *2-(4-Morpholinophenyl)quinazolin-4(3H)-one (5f)*. Off-white solid, Yield 49%. m.p. 195–197 °C. 1H NMR (400 MHz, $CDCl_3$), δ (ppm): 9.91 (1H, brs), 8.27 (1H, d, $J = 7.8$ Hz), 7.98 (2H, d, $J = 8.8$ Hz), 7.74–7.72 (2H, m), 7.41–7.37 (1H, m), 6.64 (2H, d, $J = 8.8$ Hz), 3.40–3.37 (4H, m), 2.07–2.04 (4H, m). ^{13}C NMR (100 MHz, DMSO- d_6), δ (ppm): 162.9, 152.8, 150.1, 149.8, 134.8, 129.4 (2C), 127.4 (2C), 126.2, 125.7, 120.7, 118.6, 111.6, 47.7 (2C), 25.4 (2C). HR-MS (ESI) Calcd. for $C_{18}H_{18}N_3O_2$ $[M+H]^+$: m/z 308.1399, Found 308.1398.

4.2.4.7. *2-(1H-Indol-6-yl)-5,7-dimethoxyquinazolin-4(3H)-one (5g)*. Light yellow solid, Yield 36%. m.p. 198–200 °C. 1H NMR (400 MHz, DMSO- d_6), δ (ppm): 11.93 (1H, brs), 11.45 (1H, brs), 8.29 (1H, s), 7.86 (1H, d, $J = 8.3$ Hz), 7.63 (1H, d, $J = 8.4$ Hz), 7.54 (1H, t, $J = 2.5$ Hz), 6.74 (1H, d, $J = 2.1$ Hz), 6.51–6.50 (2H, m), 3.90 (3H, s), 3.85 (3H, s). ^{13}C NMR (100 MHz, DMSO- d_6), δ (ppm): 164.7, 161.5, 160.4, 154.6, 153.8, 135.9, 130.6,

128.9, 125.3, 120.2, 118.8, 112.1, 105.0, 101.8, 101.5, 97.7, 56.4, 56.0. HR-MS (ESI) Calcd. for $C_{18}H_{16}N_3O_3$ $[M+H]^+$: m/z 323.1144, Found 322.1135.

4.2.4.8. *2-(1H-Benzo[d]imidazole-7-yl)quinazolin-4(3H)-one (5h)*. Off-white solid, Yield 35%. m.p. 174–176 °C. 1H NMR (400 MHz, DMSO- d_6), δ (ppm): 13.68 (1H, brs), 13.21 (1H, brs), 8.66 (1H, s), 8.42 (1H, d, $J = 7.6$ Hz), 8.19 (1H, d, $J = 7.8$ Hz), 7.86–7.78 (3H, m), 7.56–7.47 (2H, m). ^{13}C NMR (100 MHz, DMSO- d_6), δ (ppm): 161.4, 151.6, 149.5, 143.8, 141.0, 135.1, 129.7, 128.0, 126.9, 126.4, 126.0, 123.4, 121.8, 120.2, 116.4. HR-MS (ESI) Calcd. for $C_{15}H_{11}N_4O$ $[M+H]^+$: m/z 263.0933, Found 263.0930.

4.2.4.9. *5,7-Dimethoxy-2-(1H-pyrrolo[2,3-b]pyridin-3-yl)quinazolin-4(3H)-one (5i)*. Light white solid, Yield 51%. m.p. 185–189 °C. 1H NMR (400 MHz, DMSO- d_6), δ (ppm): 13.16 (1H, brs), 9.04 (1H, s), 8.80 (1H, d, $J = 5.5$ Hz), 8.62 (1H, d, $J = 8.1$ Hz), 7.78–7.74 (1H, m), 7.14 (1H, d, $J = 2.2$ Hz), 6.54 (1H, d, $J = 2.2$ Hz), 3.95 (3H, s), 3.87 (3H, s). ^{13}C NMR (100 MHz, DMSO- d_6), δ (ppm): 165.0, 161.6, 159.0, 151.8, 149.7, 139.6, 136.8, 132.6, 129.8, 127.4, 119.2, 104.6, 104.0, 100.8, 97.8, 56.5, 56.2. HR-MS (ESI) Calcd. for $C_{17}H_{15}N_4O_3$ $[M+H]^+$: m/z 323.1144, Found 323.1140.

4.2.4.10. *2-(1H-Pyrrolo[2,3-b]pyridin-3-yl)quinazolin-4(3H)-one (5j)*. Off-white solid, Yield 44%. m.p. 169–171 °C. 1H NMR (400 MHz, DMSO- d_6), δ (ppm): 12.60 (1H, brs), 12.38 (1H, brs), 8.60–8.57 (2H, m), 8.10 (2H, dd, $J = 6.7$ Hz, 7.1 Hz), 7.80–7.78 (1H, m), 7.65 (1H, d, $J = 7.0$ Hz), 7.44–7.37 (2H, m). ^{13}C NMR (100 MHz, DMSO- d_6), δ (ppm): 161.2, 150.3, 150.1, 143.9, 143.3, 135.0, 132.7, 129.9, 127.0, 126.5, 125.7, 121.6, 121.1, 118.3, 106.9. HR-MS (ESI) Calcd. for $C_{15}H_{11}N_4O$ $[M+H]^+$: m/z 263.0933, Found 263.0931.

4.2.4.11. *2-(1H-Benzo[d]imidazole-7-yl)-5,7-dimethoxyquinazolin-4(3H)-one (5k)*. Light yellow solid, Yield 32%. m.p. 189–191 °C. 1H NMR (400 MHz, DMSO- d_6), δ (ppm): 13.16 (2H, brs), 8.62 (1H, s), 8.34–8.33 (1H, m), 7.84 (1H, d, $J = 7.7$ Hz), 7.45–7.44 (1H, m), 6.81 (1H, d, $J = 1.9$ Hz), 6.56 (1H, d, $J = 1.9$ Hz), 3.92 (3H, s), 3.86 (3H, s). ^{13}C NMR (100 MHz, DMSO- d_6), δ (ppm): 165.0, 164.7, 161.5, 159.3, 153.4, 152.1, 143.7, 123.5, 122.2, 121.2, 117.8, 113.5, 105.4, 101.9, 98.2, 56.4, 56.1. HR-MS (ESI) Calcd. for $C_{17}H_{15}N_4O_3$ $[M+H]^+$: m/z 322.1192, Found 322.1190.

4.2.5. Preparation of compound 7

N-Boc-Piperazine (1.82 g, 9.77 mmol) was added to a 250 mL three-necked flask with mechanical stirring and a thermometer. Triethylamine (1.48 g, 14.66 mmol), dichloromethane (40 mL), cooled to 0 °C, cyclopropanecarbonyl chloride (1.12 g, 10.75 mmol) was slowly added dropwise, and the temperature was controlled from 0 to 5 °C. After the completion of the dropwise addition, the reaction was carried out for 3 h at 10–25 °C. And then added 50 mL of water, added sodium carbonate to adjust pH = 8–9, separated the liquid, collected the organic phase, added 100 mL of water phase, and extracted once with dichloromethane. The methylene chloride phases were combined, washed once with 0.05 mol/L diluted hydrochloric acid (10 mL), and once with 50 mL of water. The combined organic were dried (Na_2SO_4) and concentrated to give the last crude product 2.1 g of 4-(cyclopropanecarbonyl)piperazine-1-*N*-

Boc (Yield 82%), then 4-(cyclopropanecarbonyl)piperazine-1-*N*-Boc (2.1 g, 8.2 mmol) was added to saturated methanol hydrochloride solution (35 mL) at 0 °C and the solution was stirred for 15 min. The mixture was allowed to reach room temperature, and stirred for 4–6 h. The solvent was removed under reduced pressure, the oily residue was diluted with water and alkalified with 1 mol/L NaOH to pH = 12, extracted with ethyl acetate (3 × 50 mL). The combined organic extracts were dried (Na₂SO₄) and concentrated to give the cyclopropyl (piperazin-1-yl)methanone (compound **7**), which was used for reduction without further purification (yield 94%).

4.2.6. Preparation of compounds **10a** and **10b**

A mixture of 3-formylbenzoic acid analogue (10 mmol, 1 equiv.), thionyl chloride (12 mmol, 2.2 equiv.), and dimethylformamide (2 mL), in toluene (50 mL) was slowly warmed to 80 °C and stirred at that temperature for 3 h. The toluene was eliminated in the rotary evaporator to get 3-formylbenzoyl analogues (**9a** and **9b**) used in the next step (yield 87%–90%).

Cyclopropyl (piperazin-1-yl)methanone (5.3 mmol, 1 equiv.) was dissolved in DCM (25 mL). Triethylamine (15.9 mmol, 3 equiv.) was added and the solution was cooled at 0 °C. 3-Formylbenzoyl chloride analogue (5.3 mmol, 1 equiv., diluted with 5 mL DCM) was added dropwise and then the reaction was stirred to room temperature. After 3 h, water and DCM were added, the phases were separated and the aqueous phase was extracted twice more with DCM. The combined organics were washed with brine, dried over sodium sulfate, filtered and evaporated to a white solid. And then purification of this solid by silica gel chromatography (ethyl acetate/petroleum ether = 2:1) to give compounds **10a** and **10b** as a white solid (yield 69%–73%).

4.2.7. Preparation of target compounds **11a–e**

2-Aminobenzamide analogues (**4a–c**, 0.61 mmol, 1 equiv.) and compound intermediates (**10a** and **b**, 0.61 mmol, 1 equiv.) were dissolved in DMAc (10.0 mL) and treated with sodium hydrogen sulfite (0.74 mmol, 1.2 equiv.) and PTSA (0.15 mmol, 0.24 equiv.). The reaction mixture was stirred at 120 °C for 16–20 h. Water (80 mL) was added to the reaction, and the precipitated solid was collected by filtration, purification of this solid by silica gel chromatography (dichloromethane/methanol = 40:1–20:1) gave final compounds **11a–e** (35%–51% yield), respectively.

4.2.7.1. 2-(3-(4-(Cyclopropanecarbonyl)piperazine-1-carbonyl)phenyl)-5,7-dimethoxyquinazolin-4(3H)-one (11a). Yellow solid, Yield 35%. m.p. 260–262 °C. ¹H NMR (400 MHz, DMSO-*d*₆), δ (ppm): 12.12 (1H, brs), 8.25–8.20 (2H, m), 7.62–7.61 (2H, m), 6.78 (1H, d, *J* = 2.2 Hz), 6.56 (1H, d, *J* = 2.2 Hz), 3.89 (3H, s), 3.86 (3H, s), 3.71–3.41 (8H, m), 1.98–1.96 (1H, m), 0.75–0.71 (4H, m). ¹³C NMR (100 MHz, DMSO-*d*₆), δ (ppm): 171.8, 168.1, 164.8, 161.6, 159.5, 159.1, 153.2, 150.5, 132.5, 130.4, 122.6, 117.1, 116.8, 105.4, 101.9, 98.7, 56.5, 56.1, 53.5, 52.8, 45.1, 42.1 (2C), 10.8, 7.6 (2C). HR-MS (ESI) Calcd. for C₂₅H₂₇N₄O₅ [M+H]⁺: *m/z* 463.1981, Found 463.1980.

4.2.7.2. 2-(3-(4-(Cyclopropanecarbonyl)piperazine-1-carbonyl)phenyl)quinazolin-4(3H)-one (11b). Off-white solid, Yield 51%. m.p. 222–224 °C. ¹H NMR (400 MHz, DMSO-*d*₆), δ (ppm): 12.61 (1H, brs), 8.27 (1H, d, *J* = 7.8 Hz), 8.22 (1H, s), 8.17 (1H,

d, *J* = 7.8 Hz), 7.86–7.84 (1H, m), 7.77 (1H, d, *J* = 8.0 Hz), 7.65 (2H, d, *J* = 4.5 Hz), 7.54 (1H, t, *J* = 7.5 Hz), 3.73–3.52 (8H, m), 1.98–1.96 (1H, m), 0.76–0.72 (4H, m). ¹³C NMR (100 MHz, DMSO-*d*₆), δ (ppm): 171.8, 169.0, 162.6, 152.1, 149.0, 136.6, 135.1, 133.4, 130.2, 129.4, 129.2, 127.9, 127.2, 126.7, 126.3, 121.5, 53.5, 52.8, 45.1, 42.1, 10.8, 7.6 (2C). HR-MS (ESI) Calcd. for C₂₃H₂₃N₄O₃ [M+H]⁺: *m/z* 403.1770, Found 403.1771.

4.2.7.3. 2-(4-(4-(Cyclopropanecarbonyl)piperazin-1-yl)methyl)phenyl)-5,7-dimethoxyquinazolin-4(3H)-one (11c). Off-white solid, Yield 45%. m.p. 230–232 °C. ¹H NMR (400 MHz, DMSO-*d*₆), δ (ppm): 12.00 (1H, brs), 8.14 (2H, d, *J* = 8.2 Hz), 7.47 (2H, d, *J* = 8.2 Hz), 6.74 (1H, d, *J* = 2.2 Hz), 6.54 (1H, d, *J* = 2.2 Hz), 3.89 (3H, s), 3.85 (3H, s), 3.68 (2H, brs), 3.47 (2H, brs), 2.41–2.34 (4H, m), 1.98–1.91 (1H, m), 0.71–0.67 (4H, m). ¹³C NMR (100 MHz, DMSO-*d*₆), δ (ppm): 171.8, 164.7, 161.4, 160.2, 153.5, 153.1, 142.1, 131.5, 129.3, 128.0 (2C), 126.0, 105.2, 101.9, 101.7, 98.1, 61.8, 56.4, 56.1, 53.5, 52.8, 45.3, 42.1, 10.7, 7.4 (2C). HR-MS (ESI) Calcd. for C₂₅H₂₉N₄O₄ [M+H]⁺: *m/z* 449.2189, Found 449.2191.

4.2.7.4. 2-(4-(4-(Cyclopropanecarbonyl)piperazin-1-yl)methyl)phenyl)quinazolin-4(3H)-one (11d). Off-white solid, Yield 44%. m.p. 220–222 °C. ¹H NMR (400 MHz, DMSO-*d*₆), δ (ppm): 12.49 (1H, brs), 8.17–8.15 (3H, m), 7.84 (1H, dd, *J* = 8.4 Hz, 1.3 Hz), 7.76 (1H, d, *J* = 8.0 Hz), 7.53 (1H, d, *J* = 7.8 Hz), 7.49 (1H, d, *J* = 8.0 Hz), 3.75 (2H, s), 3.71–3.51 (8H, m), 1.96–1.93 (1H, m), 0.72–0.67 (4H, m). ¹³C NMR (100 MHz, DMSO-*d*₆), δ (ppm): 171.8, 162.7, 152.6, 149.2, 142.1, 135.1, 131.9, 130.0, 129.4, 128.1 (2C), 127.9 (2C), 127.8, 126.9, 126.3, 121.4, 61.8, 52.8, 45.3, 42.0, 10.8, 7.6 (2C). HR-MS (ESI) Calcd. for C₂₃H₂₅N₄O₂ [M+H]⁺: *m/z* 417.1927, Found 417.1928.

4.2.7.5. 2-(3-(4-(Cyclopropanecarbonyl)piperazine-1-carbonyl)phenyl)-5-methoxyquinazolin-4(3H)-one (11e). Off-white solid, Yield 48%. m.p. 218–220 °C. ¹H NMR (400 MHz, DMSO-*d*₆), δ (ppm): 12.25 (1H, brs), 8.26–8.24 (1H, m), 8.20 (1H, s), 7.72 (1H, t, *J* = 8.2 Hz), 7.62 (2H, d, *J* = 4.7 Hz), 7.28 (1H, d, *J* = 8.2 Hz), 7.03 (1H, d, *J* = 8.2 Hz), 3.89 (3H, s), 3.70–3.56 (8H, m), 1.98 (1H, s), 0.76–0.72 (4H, m). ¹³C NMR (100 MHz, DMSO-*d*₆), δ (ppm): 171.8, 169.0, 160.7, 160.2, 160.2, 152.3, 151.5, 136.6, 135.3, 133.0, 130.2, 129.3 (2C), 126.6, 119.9, 111.1, 108.9, 56.4, 52.8, 45.1, 42.2, 10.8, 7.6 (2C). HR-MS (ESI) Calcd. for C₂₄H₂₅N₄O₄ [M+H]⁺: *m/z* 433.1876, Found 433.1877.

4.2.8. Preparation of compounds **14a** and **14b**

A mixture of 3-fluoro-4-formylbenzoic acid (10 mmol, 1 equiv.), thionyl chloride (12 mmol, 2.2 equiv.), and DMF (2 mL), in toluene (50 mL) was slowly warmed to 80 °C, and stirred at that temperature for 4 h. The toluene was eliminated in the rotary evaporator to get 3-fluoro-4-formylbenzoyl chloride (compound **13**) used in the next step as such (yield 73%).

3-(Trifluoromethyl)-5,6,7,8-tetrahydro-[1,2,4]triazolo[4,3-*a*]pyrazine hydrochloride (5.3 mmol, 1 equiv.) was dissolved in DCM (25 mL), triethylamine (15.9 mmol, 3 equiv.) was added and the solution was cooled at 0 °C. 3-Fluoro-4-formylbenzoyl chloride (5.3 mmol, 1 equiv., diluted with 5 mL DCM) was added dropwise and then the reaction was stirred to room temperature. After 4 h, water and DCM were added, the phases were separated and the aqueous phase was extracted twice

more with DCM. The combined organics were washed with brine, dried over sodium sulfate, filtered and evaporated to a white solid. And then purification of this solid by silica gel chromatography (ethyl acetate/petroleum ether = 1:1) to give compound **14a** named 4-(4-(cyclopropanecarbonyl)piperazine-1-carbonyl)-2-fluorobenzaldehyde as a white solid (yield 78%).

The synthetic route of compound **14b** named 2-fluoro-4-(3-(trifluoromethyl)-5,6,7,8-tetrahydro-[1,2,4]triazolo[4,3-*a*]pyrazine-7-carbonyl)benzaldehyde was the same as that of compound **14a** (yield 64%).

4.2.9. Preparation of target compounds **15a–e**

2-Aminobenzamide analogues (0.61 mmol, 1 equiv.) and intermediates (**14a** and **14b**, 0.61 mmol, 1 equiv.) were dissolved in DMAc (8.0 mL) and treated with sodium hydrogen sulfite (0.74 mmol, 1.2 equiv.) and PTSA (0.15 mmol, 0.24 equiv.), respectively. The reaction mixture was stirred at 120 °C for 16–20 h. Water (80 mL) was added to the reaction, and the precipitated solid was collected by filtration, purification of this solid by silica gel chromatography (dichloromethane/methanol = 30:1) gave final compounds **15a–e** (37%–58% yield), respectively.

4.2.9.1. 2-(4-(4-(Cyclopropanecarbonyl)piperazine-1-carbonyl)-2-fluorophenyl)-5,7-dimethoxyquinazolin-4(3H)-one (15a). Light yellow solid, Yield 47%. m.p. 233–235 °C. ¹H NMR (400 MHz, DMSO-*d*₆), δ (ppm): 12.28 (1H, brs), 7.81 (1H, dd, *J* = 6.7 Hz, 1.8 Hz), 7.69–7.66 (1H, m), 7.46–7.44 (1H, m), 6.75 (1H, d, *J* = 2.2 Hz), 6.59 (1H, d, *J* = 2.2 Hz), 3.88 (3H, s), 3.86 (3H, s), 3.75–3.54 (8H, m), 1.27–1.24 (1H, m), 0.75–0.71 (4H, m). ¹³C NMR (100 MHz, DMSO-*d*₆), δ (ppm): 171.8, 168.1, 164.7, 161.4, 159.5, 159.1, 153.2, 150.5, 132.5 (d, *J*_{C-F} = 9.1 Hz), 132.0, 130.4, 122.6 (d, *J*_{C-F} = 13.8 Hz), 117.1, 116.8, 105.4, 101.9, 56.5, 56.4, 56.1, 54.0, 45.3, 42.3, 10.8, 7.6 (2C). HR-MS (ESI) Calcd. for C₂₅H₂₆FN₄O₅ [M+H]⁺: *m/z* 481.1887, Found 481.1886.

4.2.9.2. 2-(4-(4-(Cyclopropanecarbonyl)piperazine-1-carbonyl)-2-fluorophenyl)quinazolin-4(3H)-one (15b). Off-white solid, Yield 41%. m.p. 197–199 °C. ¹H NMR (400 MHz, DMSO-*d*₆), δ (ppm): 12.63 (1H, brs), 8.18 (1H, d, *J* = 7.9 Hz), 7.89–7.85 (2H, m), 7.75 (1H, s), 7.24 (1H, d, *J* = 7.9 Hz), 7.58 (1H, dd, *J* = 7.8, 7.2 Hz), 7.49 (1H, dd, *J* = 9.2, 8.8 Hz), 3.76–3.55 (8H, m), 1.21–1.19 (1H, m), 0.76–0.72 (4H, m). ¹³C NMR (100 MHz, DMSO-*d*₆), δ (ppm): 171.8, 168.1, 161.9, 159.1, 149.7, 149.0, 135.1, 132.2 (d, *J*_{C-F} = 9.4 Hz), 130.5, 128.0, 127.6, 126.3, 122.8 (d, *J*_{C-F} = 14.3 Hz), 121.6, 117.1, 116.8, 56.1, 54.0, 46.8, 42.3, 19.3, 10.8, 7.6 (2C). HR-MS (ESI) Calcd. for C₂₃H₂₂FN₄O₃ [M+H]⁺: *m/z* 421.1676, Found 421.1677.

4.2.9.3. 2-(2-Fluoro-4-(3-(trifluoromethyl)-5,6,7,8-tetrahydro-[1,2,4]triazolo[4,3-*a*]pyrazine-7-carbonyl)phenyl)-5,7-dimethoxyquinazolin-4(3H)-one (15c). Yellow solid, Yield 35%. m.p. 195–197 °C. ¹H NMR (400 MHz, DMSO-*d*₆), δ (ppm): 12.19 (1H, brs), 7.91 (1H, dd, *J* = 2.0 Hz, 6.8 Hz), 7.78–7.25 (1H, m), 7.52–7.48 (1H, m), 6.74 (1H, d, *J* = 2.2 Hz), 6.59 (1H, d, *J* = 2.2 Hz), 4.97 (2H, s), 4.27–4.25 (2H, m), 4.05–4.00 (2H, m), 3.87 (3H, s), 3.86 (3H, s). ¹³C NMR (100 MHz, DMSO-*d*₆), δ (ppm): 170.0, 164.8, 161.5, 159.5, 152.9, 151.1, 150.5, 132.5 (q,

*J*_{C-F} = 274.8 Hz), 131.7, 130.6, 122.5 (d, *J* = 13.9 Hz), 120.7, 117.6, 117.1 (d, *J*_{C-F} = 22.4 Hz), 105.4, 101.7, 98.7, 56.5, 52.8, 25.9, 22.8, 19.2. HR-MS (ESI) Calcd. for C₂₃H₁₉F₄N₆O₄ [M+H]⁺: *m/z* 519.1404, Found 519.1408.

4.2.9.4. 2-(2-Fluoro-4-(3-(trifluoromethyl)-5,6,7,8-tetrahydro-[1,2,4]triazolo[4,3-*a*]pyrazine-7-carbonyl)phenyl)quinazolin-4(3H)-one (15d). Off-white solid, Yield 37%. m.p. 202–204 °C. ¹H NMR (400 MHz, DMSO-*d*₆), δ (ppm): 12.66 (1H, brs), 8.18 (1H, dd, *J* = 0.8 Hz, 7.8 Hz), 7.95 (1H, dd, *J* = 1.9 Hz, 7.0 Hz), 7.87 (1H, dd, *J* = 1.9 Hz, 6.8 Hz), 7.80–7.77 (1H, m), 7.73 (1H, d, *J* = 8.0 Hz), 7.59 (1H, d, *J* = 7.9 Hz), 7.52 (1H, d, *J* = 8.7 Hz), 4.98 (2H, s), 4.27–4.25 (2H, m), 4.05–4.00 (2H, m). ¹³C NMR (100 MHz, DMSO-*d*₆), δ (ppm): 168.7, 161.9, 159.4, 151.1, 149.6, 149.6, 135.1, 131.7, 130.7, 127.9 (q, *J*_{C-F} = 274.8), 126.3, 122.9 (d, *J*_{C-F} = 8.9 Hz), 121.6, 120.3, 117.9 (d, *J*_{C-F} = 17.8 Hz), 114.9, 43.6, 22.9, 21.8. HR-MS (ESI) Calcd. for C₂₁H₁₅F₄N₆O₂ [M+H]⁺: *m/z* 459.1192, Found 459.1189.

4.2.9.5. 2-(4-(4-(Cyclopropanecarbonyl)piperazine-1-carbonyl)-2-fluorophenyl)-5-methoxyquinazolin-4(3H)-one (15e). Light yellow solid, Yield 58%. m.p. 229–231 °C. ¹H NMR (400 MHz, DMSO-*d*₆), δ (ppm): 12.28 (1H, brs), 7.81 (1H, dd, *J* = 6.7 Hz, 1.8 Hz), 7.72 (1H, m), 7.70–7.66 (1H, m), 7.47 (1H, dd, *J* = 8.8, 8.6 Hz), 7.24 (1H, d, *J* = 7.8 Hz), 7.07 (1H, d, *J* = 8.3 Hz), 3.89 (3H, s), 3.76–3.55 (8H, m), 1.21–1.17 (1H, m), 0.75–0.71 (4H, m). ¹³C NMR (100 MHz, DMSO-*d*₆), δ (ppm): 171.8, 168.1, 161.6, 160.2, 159.1, 151.5, 150.0, 135.4, 132.1 (d, *J*_{C-F} = 8.7 Hz), 131.9, 130.4, 122.6 (d, *J*_{C-F} = 13.6 Hz), 119.8, 117.0, 116.8, 111.2, 109.3, 56.4, 56.1, 54.0, 45.2, 42.3, 10.8, 7.6 (2C). HR-MS (ESI) Calcd. for C₂₄H₂₄FN₄O₃ [M+H]⁺: *m/z* 451.1782, Found 451.1783.

4.2.10. Preparation of compounds **18a–u**

1,2-Dibromoethane (45 mmol, 3 equiv.) was added to a mixture of *para*-hydroxybenzaldehyde analogue (compounds **16a–u**, 15 mmol, 1 equiv.) and potassium carbonate (24 mmol, 3 equiv.) in DMF (40 mL), and the resulting mixture was stirred vigorously at room temperature for 24 h. The mixture was poured into water (150 mL), added saturated sodium chloride (150 mL) and extracted with ethyl acetate (3 × 50 mL). The combined organic phases were washed with saturated sodium chloride (100 mL), dried over Na₂SO₄ and evaporated *in vacuo* to afford compounds **17a–h** (85%–96% yield), respectively. Hydroxyl-substituted compounds (10 mmol, 1 equiv.) was added to a mixture of chemical intermediate and potassium carbonate (30 mmol, 3 equiv.) in DMF (35 mL), and the resulting mixture was stirred vigorously at room temperature overnight, or heat at 80 °C for about 8 h. The mixture was poured into water (80 mL), added saturated sodium chloride (80 mL) and extracted with ethyl acetate (3 × 50 mL). The combined organic phases were washed with saturated sodium chloride (100 mL), dried over Na₂SO₄ and evaporated *in vacuo* to afford chemical intermediate as solid to obtain compounds **18a–u** (76%–87% yield).

4.2.11. Preparation of target compounds **19a–u**

2-Amino-4,6-dimethoxybenzamide (0.61 mmol, 1 equiv.) and compound intermediates (**18a–u**) (0.61 mmol, 1 equiv.) were dissolved in DMAc (8.0 mL) and treated with sodium hydrogen

sulfite (0.74 mmol, 1.2 equiv.) and PTSA (0.15 mmol, 0.24 equiv.). The reaction mixture was stirred at 120 °C for 16–20 h. Water (80 mL) was added to the reaction, and the precipitated solid was collected by filtration, purification of this solid by silica gel chromatography (dichloromethane/methanol = 50:1–20:1) gave final compounds **19a–u** (17%–56% yield), respectively.

4.2.11.1. 2-(2-(4-Chloro-2-(5,7-dimethoxy-4-oxo-3,4-dihydroquinazolin-2-yl)phenoxy)ethoxy)benzamide (**19a**). Off-white solid, Yield 23%. m.p. 231–233 °C. ¹H NMR (400 MHz, DMSO-*d*₆), δ (ppm): 11.99 (1H, brs), 8.08 (1H, d, *J* = 5.6 Hz), 8.06 (1H, s), 7.86 (1H, dd, *J* = 7.6 Hz, 1.7 Hz), 7.50 (1H, dd, *J* = 8.3 Hz, 1.7 Hz), 7.42–7.41 (1H, m), 7.23 (1H, d, *J* = 8.3 Hz), 7.08–7.07 (1H, m), 6.74 (1H, d, *J* = 2.2 Hz), 6.53 (1H, d, *J* = 2.2 Hz), 4.60–4.52 (4H, m), 3.89 (3H, s), 3.85 (3H, s). ¹³C NMR (100 MHz, DMSO-*d*₆), δ (ppm): 166.7, 164.6, 161.3, 159.2, 156.6, 155.8, 153.4, 151.7, 132.7, 131.2, 130.2, 125.2, 124.4, 123.7, 121.4, 115.8, 113.8, 105.4, 101.8, 98.4, 68.3, 67.8, 56.4, 56.1. HR-MS (ESI) Calcd. for C₂₅H₂₃ClN₃O₆ [M+H]⁺: *m/z* 496.1275, Found 496.1270.

4.2.11.2. 2-(3-(4-Chloro-2-(5,7-dimethoxy-4-oxo-3,4-dihydroquinazolin-2-yl)phenoxy)propoxy)benzamide (**19b**). Off-white solid, Yield 31%. m.p. 195–197 °C. ¹H NMR (400 MHz, DMSO-*d*₆), δ (ppm): 11.69 (1H, brs), 7.75–7.73 (2H, m), 7.70 (1H, d, *J* = 2.7 Hz), 7.55 (2H, dd, *J* = 8.9 Hz, 2.9 Hz), 7.39–7.34 (1H, m), 7.22 (1H, d, *J* = 8.4 Hz), 6.73 (1H, d, *J* = 2.2 Hz), 6.55 (1H, d, *J* = 2.2 Hz), 4.28–4.22 (4H, m), 2.24–2.21 (2H, m), 3.86 (3H, s), 3.84 (3H, s). ¹³C NMR (100 MHz, DMSO-*d*₆), δ (ppm): 167.0, 164.6, 161.4, 159.2, 156.6, 155.8, 153.5, 152.1, 132.7, 132.6, 132.0, 130.0, 124.7, 123.9, 121.0, 120.9, 115.2, 113.4, 105.4, 101.8, 98.3, 66.2, 65.9, 56.4, 56.1, 28.8. HR-MS (ESI) Calcd. for C₂₆H₂₅ClN₃O₆ [M+H]⁺: *m/z* 510.1432, Found 510.1434.

4.2.11.3. 2-(4-(4-Chloro-2-(5,7-dimethoxy-4-oxo-3,4-dihydroquinazolin-2-yl)phenoxy)butoxy)benzamide (**19c**). Off-white solid, Yield 21%. m.p. 184–186 °C. ¹H NMR (400 MHz, DMSO-*d*₆), δ (ppm): 11.60 (1H, brs), 7.77–7.74 (1H, m), 7.55 (1H, dd, *J* = 8.8 Hz, 2.7 Hz), 7.39–7.35 (1H, m), 7.22 (1H, d, *J* = 8.9 Hz), 7.04 (1H, d, *J* = 8.1 Hz), 7.01–6.98 (1H, m), 6.74 (1H, d, *J* = 2.2 Hz), 6.55 (1H, d, *J* = 2.2 Hz), 4.18–4.10 (4H, m), 3.87 (3H, s), 3.84 (3H, s), 1.96–1.89 (4H, m). ¹³C NMR (100 MHz, DMSO-*d*₆), δ (ppm): 166.9, 164.7, 161.4, 159.1, 156.9, 156.9, 153.5, 152.0, 132.8, 132.1, 131.1, 129.9, 124.6, 124.2, 123.3, 120.8, 115.4, 113.4, 105.3, 101.8, 98.3, 68.9, 68.5, 56.4, 56.1, 26.8, 26.5. HR-MS (ESI) Calcd. for C₂₇H₂₇ClN₃O₆ [M+H]⁺: *m/z* 524.1588, Found 524.1586.

4.2.11.4. 2-(2-(4-(5,7-Dimethoxy-4-oxo-3,4-dihydroquinazolin-2-yl)phenoxy)ethoxy)benzamide (**19d**). Pure white solid, Yield 45%. m.p. 282–284 °C. ¹H NMR (400 MHz, DMSO-*d*₆), δ (ppm): 11.92 (1H, brs), 8.17 (1H, d, *J* = 8.9 Hz), 7.87 (2H, d, *J* = 8.8 Hz), 7.50–7.49 (1H, m), 7.24 (1H, d, *J* = 7.8 Hz), 7.13 (2H, d, *J* = 8.8 Hz), 7.09–7.07 (1H, m), 6.72 (1H, d, *J* = 2.2 Hz), 6.51 (1H, d, *J* = 2.2 Hz), 4.51–4.49 (4H, m), 3.89 (3H, s), 3.84 (3H, s). ¹³C NMR (100 MHz, DMSO-*d*₆), δ (ppm): 167.2, 165.5, 162.2, 162.0, 161.1, 157.6, 154.4, 133.9, 132.3, 131.2, 130.7, 126.2, 124.0, 123.3, 122.4, 115.8, 114.9, 105.8, 102.4, 98.7, 68.5,

67.6, 57.2, 56.8. HR-MS (ESI) Calcd. for C₂₅H₂₄N₃O₆ [M+H]⁺: *m/z* 462.1665, Found 462.1664.

4.2.11.5. 2-((5-(4-Chloro-2-(5,7-dimethoxy-4-oxo-3,4-dihydroquinazolin-2-yl)phenoxy)pentyl)oxy)benzamide (**19e**). Off-white solid, Yield 17%. m.p. 189–191 °C. ¹H NMR (400 MHz, DMSO-*d*₆), δ (ppm): 11.56 (1H, brs), 7.76 (1H, d, *J* = 2.8 Hz), 7.55 (2H, dd, *J* = 8.9 Hz, 2.8 Hz), 7.47–7.41 (2H, m), 7.22 (1H, d, *J* = 8.9 Hz), 7.08 (1H, d, *J* = 8.0 Hz), 6.75 (1H, d, *J* = 2.2 Hz), 6.54 (1H, d, *J* = 2.2 Hz), 4.06–4.15 (4H, m), 3.86 (3H, s), 3.83 (3H, s), 1.87–1.78 (4H, m), 1.67–1.64 (2H, m). ¹³C NMR (100 MHz, DMSO-*d*₆), δ (ppm): 166.8, 164.7, 161.4, 159.1, 156.9, 156.1, 153.5, 152.0, 132.9, 131.1, 129.8, 129.6, 124.6, 124.2, 123.3, 120.8, 115.4, 113.4, 105.4, 101.8, 98.3, 69.2, 68.9, 56.4, 56.1, 26.8, 26.5, 22.4. HR-MS (ESI) Calcd. for C₂₈H₂₉ClN₃O₆ [M+H]⁺: *m/z* 538.1745, Found 538.1744.

4.2.11.6. 2-(2-(4-(5,7-Dimethoxy-4-oxo-3,4-dihydroquinazolin-2-yl)-2,6-dimethylphenoxy)ethoxy)benzamide (**19f**). A white solid, Yield 51%. m.p. 271–273 °C. ¹H NMR (400 MHz, DMSO-*d*₆), δ (ppm): 11.83 (1H, brs), 7.89 (1H, d, *J* = 6.6 Hz), 7.69 (2H, d, *J* = 8.2 Hz), 7.50 (1H, td, *J* = 8.4 Hz, 1.6 Hz), 7.23 (1H, d, *J* = 8.2 Hz), 7.08 (1H, dd, *J* = 7.3 Hz, 7.6 Hz), 6.74 (1H, d, *J* = 2.2 Hz), 6.52 (1H, d, *J* = 2.2 Hz), 4.47–4.24 (4H, m), 3.89 (3H, s), 3.84 (3H, s), 2.30(6H, s). ¹³C NMR (100 MHz, DMSO-*d*₆), δ (ppm): 166.5, 164.7, 161.4, 160.2, 158.3, 156.8, 154.9, 153.6, 152.9, 133.1, 131.6, 131.2 (2C), 128.8, 128.1, 123.1, 121.4, 113.6, 105.1, 101.6, 98.0, 70.5, 68.5, 56.4, 56.1, 16.7 (2C). HR-MS (ESI) Calcd. for C₂₇H₂₈N₃O₆ [M+H]⁺: *m/z* 490.1978, Found 490.1974.

4.2.11.7. 2-(2-(4-(5,7-Dimethoxy-4-oxo-3,4-dihydroquinazolin-2-yl)-2,6-dimethoxyphenoxy)ethoxy)benzamide (**19g**). Pale yellow solid, Yield 26%. m.p. 271–273 °C. ¹H NMR (400 MHz, DMSO-*d*₆), δ (ppm): 11.92 (1H, brs), 7.97 (1H, dd, *J* = 7.7 Hz, 1.7 Hz), 7.76 (1H, s), 7.63 (1H, s), 7.49 (1H, td, *J* = 8.4 Hz, 1.7 Hz), 7.17 (1H, d, *J* = 8.2 Hz), 7.07–7.05 (1H, m), 6.75 (1H, d, *J* = 2.2 Hz), 6.53 (1H, d, *J* = 2.2 Hz), 4.35 (4H, s), 3.89 (3H, s), 3.85 (3H, s), 3.83 (6H, s). ¹³C NMR (100 MHz, DMSO-*d*₆), δ (ppm): 166.4, 164.7, 161.4, 160.2, 157.1, 153.4, 153.4, 152.7, 138.7, 133.2, 131.8, 128.2, 122.5, 121.2, 115.2, 113.4, 105.5, 105.5, 105.1, 101.7, 98.2, 70.9, 68.3, 56.6 (2C), 56.4, 56.1. HR-MS (ESI) Calcd. for C₂₇H₂₈N₃O₈ [M+H]⁺: *m/z* 522.1876, Found 522.1873.

4.2.11.8. 2-(2-(4-(5,7-Dimethoxy-4-oxo-3,4-dihydroquinazolin-2-yl)-2-fluorophenoxy)ethoxy)benzamide (**19h**). Off-white solid, Yield 42%. m.p. 210–212 °C. ¹H NMR (400 MHz, DMSO-*d*₆), δ (ppm): 11.92 (1H, brs), 7.77 (1H, d, *J* = 2.7 Hz), 7.74 (1H, dd, *J* = 7.7 Hz, 1.7 Hz), 7.58 (1H, dd, *J* = 8.9 Hz, 1.7 Hz), 7.51 (1H, s), 7.36 (1H, td, *J* = 8.4 Hz, 1.7 Hz), 7.14 (1H, d, *J* = 8.2 Hz), 6.99–6.97 (1H, m), 6.73 (1H, d, *J* = 2.2 Hz), 6.54 (1H, d, *J* = 2.2 Hz), 4.52–4.46 (4H, m), 3.85 (3H, s), 3.82 (3H, s). ¹³C NMR (100 MHz, DMSO-*d*₆), δ (ppm): 166.7, 164.6, 161.4, 159.2, 156.6, 155.8, 153.4, 151.8, 132.7, 132.1, 131.2, 130.2, 125.2 (d, *J*_{C-F} = 8.2 Hz), 124.4, 123.7, 121.4, 115.8 (d, *J*_{C-F} = 19.4 Hz), 113.8, 105.4, 101.8, 98.4, 68.3, 67.8, 56.4, 56.1. HR-MS (ESI) Calcd. for C₂₆H₂₃FN₃O₆ [M+H]⁺: *m/z* 480.1571, Found 480.1568.

4.2.11.9. 2-(4-(2-((1*H*-Benzo[*d*][1,2,3]triazol-1-yl)oxy)ethoxy)-3,5-dimethylphenyl)-5,7-dimethoxyquinazolin-4(3*H*)-one

(19i). Off-white solid, Yield 38%. m.p. 186–188 °C. ^1H NMR (400 MHz, DMSO- d_6), δ (ppm): 11.85 (1H, brs), 8.10 (1H, d, $J = 8.4$ Hz), 7.93 (2H, s), 7.87 (1H, d, $J = 8.4$ Hz), 7.66 (1H, dd, $J = 7.3$ Hz, 7.9 Hz), 7.49 (1H, dd, $J = 7.9$ Hz, 7.6 Hz), 6.74 (1H, d, $J = 2.2$ Hz), 6.52 (1H, d, $J = 2.2$ Hz), 4.92–4.90 (2H, m), 4.29–4.27 (2H, m), 3.89 (3H, s), 3.85 (3H, s), 2.36 (6H, s). ^{13}C NMR (100 MHz, DMSO- d_6), δ (ppm): 164.7, 161.4, 160.2, 158.4, 153.5, 152.9, 143.2, 131.2, 131.1, 129.0, 128.8 (2C), 128.1, 127.4, 125.5, 120.2, 109.7, 105.1, 101.6, 98.1, 80.6, 69.7, 56.4, 56.1, 16.7 (2C). HR-MS (ESI) Calcd. for $\text{C}_{26}\text{H}_{26}\text{N}_5\text{O}_5$ $[\text{M}+\text{H}]^+$: m/z 488.1934, Found 488.1933.

4.2.11.10. 2-(4-(2-((1H-Benzod[*d*][1,2,3]triazol-1-yl)oxy)ethoxy)-3,5-dimethoxyphenyl)-5,7-dimethoxyquinazolin-4(3H)-one (19j). Pale white solid powder, Yield 34%. m.p. 222–224 °C. ^1H NMR (400 MHz, DMSO- d_6), δ (ppm): 12.04 (1H, brs), 8.08 (1H, d, $J = 8.4$ Hz), 7.91 (1H, d, $J = 8.4$ Hz), 7.66 (1H, dd, $J = 7.4$ Hz, 7.9 Hz), 7.58 (2H, s), 7.48 (1H, dd, $J = 7.4$ Hz, 7.9 Hz), 6.76 (1H, d, $J = 2.2$ Hz), 6.53 (1H, d, $J = 2.2$ Hz), 4.84 (2H, t, $J = 3.4$ Hz), 4.35 (2H, t, $J = 3.4$ Hz), 3.90 (9H, s), 3.86 (3H, s). ^{13}C NMR (100 MHz, DMSO- d_6), δ (ppm): 164.7, 161.4, 160.9, 160.3, 153.4, 153.1, 152.6, 143.2, 139.2, 128.8 (2C), 127.7, 125.4 (2C), 120.1, 109.6, 105.5 (2C), 105.2, 101.7, 98.2, 80.8, 70.2, 56.6, 56.4, 56.1. HR-MS (ESI) Calcd. for $\text{C}_{26}\text{H}_{26}\text{N}_5\text{O}_7$ $[\text{M}+\text{H}]^+$: m/z 520.1832, Found 520.1828.

4.2.11.11. 2-(4-(2-((1H-Benzod[*d*][1,2,3]triazol-1-yl)oxy)ethoxy)phenyl)-5,7-dimethoxyquinazolin-4(3H)-one (19k). Off-white solid, Yield 48%. m.p. 233–235 °C. ^1H NMR (400 MHz, DMSO- d_6), δ (ppm): 11.92 (1H, brs), 8.17 (2H, d, $J = 8.7$ Hz), 8.09 (1H, d, $J = 8.4$ Hz), 7.29 (1H, d, $J = 8.4$ Hz), 7.60 (1H, dd, $J = 7.4$ Hz, 7.8 Hz), 7.46 (1H, dd, $J = 7.9$ Hz, 7.4 Hz), 7.03 (2H, d, $J = 8.7$ Hz), 6.73 (1H, d, $J = 2.2$ Hz), 6.51 (1H, d, $J = 2.2$ Hz), 4.96–4.46 (4H, m), 3.89 (3H, s), 3.84 (3H, s). ^{13}C NMR (100 MHz, DMSO- d_6), δ (ppm): 164.7, 161.4, 160.9, 160.0, 153.6, 152.8, 143.2, 129.8 (2C), 128.9, 127.1, 125.4, 125.3, 120.2, 114.8 (2C), 109.6, 105.0, 101.6, 97.9, 79.3, 65.8, 56.4, 56.1. HR-MS (ESI) Calcd. for $\text{C}_{24}\text{H}_{22}\text{N}_5\text{O}_5$ $[\text{M}+\text{H}]^+$: m/z 460.1621, Found 460.1607.

4.2.11.12. 2-(4-(2-((1H-Benzod[*d*][1,2,3]triazol-1-yl)oxy)ethoxy)-3-fluorophenyl)-5,7-dimethoxyquinazolin-4(3H)-one (19l). Off-white solid, Yield 32%. m.p. 233–236 °C. ^1H NMR (400 MHz, DMSO- d_6), δ (ppm): 11.99 (1H, brs), 8.09–8.04 (3H, m), 7.81 (1H, d, $J = 8.3$ Hz), 7.60 (1H, dd, $J = 7.2$ Hz, 8.0 Hz), 7.46 (1H, dd, $J = 8.0$ Hz, 7.4 Hz), 7.36–7.34 (1H, m), 6.74 (1H, d, $J = 2.2$ Hz), 6.53 (1H, d, $J = 2.2$ Hz), 4.99–4.98 (2H, m), 4.56–4.54 (2H, m), 3.89 (3H, s), 3.85 (3H, s). ^{13}C NMR (100 MHz, DMSO- d_6), δ (ppm): 164.7, 161.4, 160.1, 153.3, 152.8, 151.7, 148.9 (d, $J_{\text{C-F}} = 10.8$ Hz), 143.2, 129.0, 128.9, 127.6, 125.9, 125.0, 120.2, 116.7 (d, $J_{\text{C-F}} = 18.9$ Hz), 114.9, 109.4, 105.1, 101.7, 98.1, 79.1, 66.8, 56.4, 56.1. HR-MS (ESI) Calcd. for $\text{C}_{24}\text{H}_{21}\text{FN}_5\text{O}_5$ $[\text{M}+\text{H}]^+$: m/z 478.1526, Found 478.1529.

4.2.11.13. 2-(4-(2-((1H-Indazol-6-yl)oxy)ethoxy)-3,5-dimethylphenyl)-5,7-dimethoxyquinazolin-4(3H)-one (19m). Off-white solid, Yield 34%. m.p. 221–223 °C. ^1H NMR (400 MHz, DMSO- d_6), δ (ppm): 12.91 (1H, brs), 11.83 (1H, brs), 7.95 (1H, s), 7.91 (2H, s), 7.47 (1H, d, $J = 8.9$ Hz), 7.24 (1H, s),

7.05 (1H, dd, $J = 8.9$ Hz, 2.0 Hz), 6.74 (1H, d, $J = 2.2$ Hz), 6.52 (1H, d, $J = 2.2$ Hz), 4.31–4.30 (2H, m), 4.22–4.21 (2H, m), 3.89 (3H, s), 3.84 (3H, s), 2.33 (6H, s). ^{13}C NMR (100 MHz, DMSO- d_6), δ (ppm): 164.7, 161.4, 160.1, 158.6, 153.6 (2C), 152.9, 139.6, 136.3, 133.3, 131.2 (2C), 128.7, 123.5, 118.6, 111.6, 105.1, 101.6, 101.3, 100.9, 98.1, 71.3, 67.9, 56.4, 56.1, 16.6 (2C). HR-MS (ESI) Calcd. for $\text{C}_{27}\text{H}_{27}\text{N}_4\text{O}_5$ $[\text{M}+\text{H}]^+$: m/z 487.1981, Found 487.1988.

4.2.11.14. 2-(4-(2-((1H-Indazol-6-yl)oxy)ethoxy)-3,5-dimethoxyphenyl)-5,7-dimethoxyquinazolin-4(3H)-one (19n). Off-white solid, Yield 30%. m.p. 260–262 °C. ^1H NMR (400 MHz, DMSO- d_6), δ (ppm): 12.89 (1H, brs), 12.03 (1H, brs), 7.94 (1H, s), 7.55 (2H, s), 7.45 (1H, d, $J = 8.9$ Hz), 7.19 (1H, s), 7.05 (1H, dd, $J = 8.9$ Hz, 2.0 Hz), 6.76 (1H, d, $J = 2.2$ Hz), 6.53 (1H, d, $J = 2.2$ Hz), 4.32–4.30 (2H, m), 4.25–4.23 (2H, m), 3.90 (3H, s), 3.86 (9H, s). ^{13}C NMR (100 MHz, DMSO- d_6), δ (ppm): 164.7, 161.4, 160.9, 159.4, 153.4, 153.2, 152.8, 139.7, 136.2, 133.3, 131.1, 129.9, 123.5, 118.8, 111.4, 105.6 (2C), 105.1, 101.7, 101.4, 98.2, 71.5, 68.2, 56.6 (2C), 56.4, 56.1. HR-MS (ESI) Calcd. for $\text{C}_{27}\text{H}_{27}\text{N}_4\text{O}_7$ $[\text{M}+\text{H}]^+$: m/z 519.1879, Found 519.1877.

4.2.11.15. 2-(4-(2-((1H-Indazol-6-yl)oxy)ethoxy)phenyl)-5,7-dimethoxyquinazolin-4(3H)-one (19o). Light yellow solid, Yield 34%. m.p. 255–257 °C. ^1H NMR (400 MHz, DMSO- d_6), δ (ppm): 12.91 (1H, brs), 11.92 (1H, brs), 8.18 (2H, d, $J = 8.9$ Hz), 7.95 (1H, s), 7.45 (1H, d, $J = 8.8$ Hz), 7.26 (1H, d, $J = 1.9$ Hz), 7.13 (2H, d, $J = 8.9$ Hz), 7.06 (1H, dd, $J = 8.9$ Hz, 2.2 Hz), 6.72 (1H, d, $J = 2.2$ Hz), 6.51 (1H, d, $J = 2.2$ Hz), 4.45–4.43 (2H, m), 4.37–4.35 (2H, m), 3.89 (3H, s), 3.84 (3H, s). ^{13}C NMR (100 MHz, DMSO- d_6), δ (ppm): 164.7, 161.4, 161.7, 159.4, 154.4, 153.4, 153.0, 152.7, 139.7, 136.2, 133.2, 131.0, 127.8, 123.5, 118.8, 111.6, 105.6, 105.1, 101.6, 101.4, 97.9, 79.3, 65.8, 56.4, 56.1. HR-MS (ESI) Calcd. for $\text{C}_{25}\text{H}_{23}\text{N}_4\text{O}_5$ $[\text{M}+\text{H}]^+$: m/z 459.1668, Found 459.1668.

4.2.11.16. 2-(4-(2-((1H-Benzod[*d*][1,2,3]triazol-1-yl)oxy)ethoxy)-3-chlorophenyl)-5,7-dimethoxyquinazolin-4(3H)-one (19p). Off-white solid, Yield 34%. m.p. 270–273 °C. ^1H NMR (400 MHz, DMSO- d_6), δ (ppm): 11.97 (1H, brs), 8.09–8.03 (3H, m), 7.78 (1H, d, $J = 8.3$ Hz), 7.62–7.58 (1H, m), 7.48–7.44 (1H, m), 7.34 (1H, dd, $J = 8.7$ Hz, 8.4 Hz), 6.75 (1H, d, $J = 2.2$ Hz), 6.53 (1H, d, $J = 2.2$ Hz), 4.99–4.97 (2H, m), 4.56–4.54 (2H, m), 3.89 (3H, s), 3.85 (3H, s). ^{13}C NMR (100 MHz, DMSO- d_6), δ (ppm): 164.7, 161.4, 160.2, 158.4, 153.3, 151.7, 148.9, 131.2, 131.1, 129.0, 128.8 (2C), 128.1, 127.4, 125.5, 120.2, 109.7, 105.1, 101.6, 98.2, 79.1, 66.8, 56.4, 56.1. HR-MS (ESI) Calcd. for $\text{C}_{24}\text{H}_{21}\text{ClN}_5\text{O}_5$ $[\text{M}+\text{H}]^+$: m/z 478.1527, Found 478.1524.

4.2.11.17. 2-(2-(2-((3a,7a-Dihydro-1H-benzod[*d*][1,2,3]triazol-1-yl)oxy)ethoxy)-4-methoxyphenyl)-5,7-dimethoxyquinazolin-4(3H)-one (19q). Off-white solid, Yield 32%. m.p. 216–219 °C. ^1H NMR (400 MHz, DMSO- d_6), δ (ppm): 11.39 (1H, brs), 7.98–7.96 (1H, m), 7.82 (1H, d, $J = 8.6$ Hz), 7.64–7.62 (1H, m), 6.76–6.72 (2H, m), 6.71 (1H, d, $J = 2.2$ Hz), 6.52 (1H, d, $J = 2.2$ Hz), 4.95–4.93 (2H, m), 4.55–4.53 (2H, m), 3.88 (3H, s), 3.84 (6H, s). ^{13}C NMR (100 MHz, DMSO- d_6), δ (ppm): 164.5, 163.2, 161.4, 159.2, 157.9, 153.8, 152.8, 143.1, 132.3, 128.7,

127.4, 125.3, 120.0, 115.0, 109.4 (2C) 107.0, 105.2, 101.6, 100.0, 97.9, 79.2, 66.3, 56.4, 56.1. HR-MS (ESI) Calcd. for $C_{25}H_{26}N_5O_6$ $[M+H]^+$: m/z 490.1727, Found 490.1720.

4.2.11.18. 2-(4-Chloro-2-(2-((3*a*,7*a*-dihydro-1*H*-benzo[*d*][1,2,3]triazol-1-yl)oxy)ethoxy)phenyl)-5,7-dimethoxyquinazolin-4(3*H*)-one (**19r**). Off-white solid, Yield 46%. m.p. 215–217 °C. 1H NMR (400 MHz, DMSO- d_6), δ (ppm): 11.74 (1H, brs), 7.5–7.94 (1H, m), 7.73 (1H, d, $J = 2.7$ Hz), 7.59–7.53 (2H, m), 7.35–7.29 (2H, m), 7.26 (1H, d, $J = 8.9$ Hz), 6.77 (1H, d, $J = 2.2$ Hz), 6.59 (1H, d, $J = 2.2$ Hz), 4.93–4.89 (2H, m), 4.50–4.49 (2H, m), 3.88 (3H, s), 3.87 (3H, s). ^{13}C NMR (100 MHz, DMSO- d_6), δ (ppm): 164.4, 161.4, 159.2, 155.3, 153.5, 151.9, 143.1, 132.0, 130.2, 128.6, 127.3, 125.3, 125.2, 124.8, 120.0, 115.4, 109.2, 105.6, 101.8, 98.4, 79.2, 66.6, 56.4, 56.1. HR-MS (ESI) Calcd. for $C_{24}H_{23}ClN_5O_5$ $[M+H]^+$: m/z 494.1231, Found 494.1234.

4.2.11.19. 2-(2-(2-(5,7-Dimethoxy-4-oxo-3,4-dihydroquinazolin-2-yl)-4-fluorophenoxy)ethoxy)benzamide (**19s**). Off-white solid, Yield 58%. m.p. 245–247 °C. 1H NMR (400 MHz, DMSO- d_6), δ (ppm): 11.74 (1H, brs), 7.83 (1H, d, $J = 8.6$ Hz), 7.76 (1H, dd, $J = 8.9$ Hz, 2.2 Hz), 7.47 (1H, d, $J = 2.9$ Hz), 7.41–7.35 (1H, m), 6.72 (1H, dd, $J = 8.9$, 2.2 Hz), 7.18 (1H, d, $J = 8.2$ Hz), 7.01 (1H, t, $J = 7.6$ Hz), 6.81 (1H, d, $J = 2.2$ Hz), 6.50 (1H, d, $J = 2.2$ Hz), 4.56–4.51 (4H, m), 3.86 (3H, s), 3.85 (3H, s). ^{13}C NMR (100 MHz, DMSO- d_6), δ (ppm): 166.7, 163.1, 161.4, 158.2, 157.9, 156.7, 149.9, 144.1, 132.7, 132.2, 131.2, 131.3, 129.4 (d, $J_{C-F} = 9.2$ Hz), 124.4, 123.7, 121.9, 121.4, 115.2 (d, $J_{C-F} = 19.7$ Hz), 113.9, 107.1, 106.2, 100.1, 67.9, 67.8, 56.1, 55.9. HR-MS (ESI) Calcd. for $C_{25}H_{23}FN_3O_6$ $[M+H]^+$: m/z 480.1571, Found 480.1570.

4.2.11.20. 5,7-Dimethoxy-2-(4-(2-((4-oxo-3,4-dihydroquinazolin-6-yl)oxy)ethoxy)phenyl)quinazolin-4(3*H*)-one (**19t**). Off-white solid, Yield 48%. m.p. 281–283 °C. 1H NMR (400 MHz, DMSO- d_6), δ (ppm): 11.91 (1H, brs), 10.13 (1H, brs), 8.23 (1H, s), 8.14 (2H, d, $J = 8.9$ Hz), 7.55 (1H, d, $J = 8.7$ Hz), 7.44 (1H, d, $J = 2.8$ Hz), 7.28 (1H, dd, $J = 8.7$, 2.8 Hz), 7.07 (2H, d, $J = 8.9$ Hz), 6.71 (1H, d, $J = 2.2$ Hz), 6.50 (1H, d, $J = 2.2$ Hz), 4.39–4.37 (4H, m), 3.88 (3H, s), 3.83 (3H, s). ^{13}C NMR (100 MHz, DMSO- d_6), δ (ppm): 164.7, 161.4, 161.0, 160.5, 160.2, 156.9, 153.6, 152.8, 145.7, 141.6, 129.9 (2C), 129.3, 125.3, 124.3, 122.9, 114.9 (2C), 109.3, 105.0, 101.5, 97.9, 65.8, 56.4, 56.0, 45.6. HR-MS (ESI) Calcd. for $C_{26}H_{23}N_4O_6$ $[M+H]^+$: m/z 484.1439, Found 484.1437.

4.2.11.21. 4-(2-(4-(5,7-Dimethoxy-4-oxo-3,4-dihydroquinazolin-2-yl)phenoxy)ethoxy)nicotinamide (**19u**). Off-white solid, Yield 21%. m.p. 275–277 °C. 1H NMR (400 MHz, DMSO- d_6), δ (ppm): 11.91 (1H, brs), 8.17 (2H, d, $J = 8.8$ Hz), 7.86 (1H, d, $J = 6.3$ Hz), 7.50 (1H, t, $J = 7.2$ Hz), 7.23 (1H, d, $J = 8.2$ Hz), 7.12 (2H, d, $J = 8.8$ Hz), 7.09–7.05 (1H, m), 6.71 (1H, d, $J = 2.2$ Hz), 6.50 (1H, d, $J = 2.2$ Hz), 4.50–4.45 (4H, m), 3.89 (3H, s), 3.84 (3H, s). ^{13}C NMR (100 MHz, DMSO- d_6), δ (ppm): 166.7, 164.6, 161.4, 159.2, 156.7, 155.8, 153.4, 151.8, 132.7, 131.2, 130.2, 125.2, 124.4, 123.7, 121.4, 115.8, 113.8, 105.4, 101.8, 98.4, 68.3, 67.8, 57.4, 57.1. HR-MS (ESI) Calcd. for $C_{24}H_{23}N_4O_6$ $[M+H]^+$: m/z 463.1618, Found 463.1615.

4.2.11.22. 2-((4-(5,7-Dimethoxy-4-oxo-3,4-dihydroquinazolin-2-yl)phenoxy)methoxy)benzamide (**19v**). Pure white solid, Yield 42%. m.p. 266–268 °C. 1H NMR (400 MHz, DMSO- d_6), δ (ppm):

12.07 (1H, brs), 8.19 (1H, d, $J = 8.1$ Hz), 7.86 (1H, dd, $J = 7.6$, 1.5 Hz), 7.65–7.63 (3H, m), 7.55 (1H, s), 7.46–7.43 (1H, m), 7.19 (1H, d, $J = 8.1$ Hz), 7.05–7.02 (1H, m), 6.75 (1H, d, $J = 2.2$ Hz), 6.55 (1H, d, $J = 2.2$ Hz), 5.35 (2H, s), 3.89 (3H, s), 3.85 (3H, s). ^{13}C NMR (100 MHz, DMSO- d_6), δ (ppm): 167.0, 164.7, 161.4, 160.2, 156.3, 155.1, 153.4, 153.0, 140.6, 132.6, 132.4, 131.0, 128.3, 128.0, 124.3, 121.3, 113.8, 113.6, 105.3, 101.8, 98.3, 68.8, 56.4, 56.1.

4.3.3. Bioinformatics analysis

BRD4-related and PARP1-related PPI network was predicted by PrePPI (<https://honiglab.c2b2.columbia.edu/PrePPI/>). Then, function annotation of BRD4-related and PARP1-related proteins were performed using DAVID (<https://david.ncifcrf.gov/>), and the proteins with the functions of cell cycle and apoptosis were filtered out. Finally, the correlation between BRD4 and PARP1 in *BRCA* tumor, which represents invasive breast cancer in TCGA, was analyzed using “correlation analysis” section in GEPIA (<http://gepia.cancer-pku.cn/>) by given sets of TCGA expression data⁷¹. The specific process was that entered the names of the two targets, selected the specific tissue, and used Spearman method to calculate the correlation coefficient, and finally clicked “plot” to generate the corresponding scatter plot. PPI networks were produced by using Cytoscape_v3.7.2.

4.4. Molecular docking

The combinatorial compound database was constructed in the design and enumerate module of Accelrys Discovery Studio (version 3.5; San Diego, CA, USA). Then all the generated combinatorial compounds were filtered by the Lipinski’s rule of five and prepared with pH from 6.5 to 8.5 for the following docking. The crystal structures of BRD4(BD1), BRD4(BD2) and PARP1 were derived from Protein Data Bank database (PDB, <https://www.rcsb.org/>) with PDB IDs of 4MR4, 5UOO and 5DS3. The centroids of the native ligands in all crystal structures were defined as the centers of binding pockets in docking process. According to the docking protocol⁷², five converse water molecules of BRD4(BD1) and BRD4(BD2) complex were retained, while all the water molecules were deleted in the PARP1 complex. We employed the CDocker protocol as docking approaches to carry out semiflexible docking. We set other parameters as default values.

4.5. Pharmacology

4.5.1. PARP1 inhibition assays

The inhibition of the tested compounds on PARP1 enzymatic activity was determined by enzyme linked immunosorbent assay (ELISA) in 96-well plates. The inhibition rate of PARP1 enzymatic activity was calculated as (Lu control – Lu treated/Lu control) \times 100%. The PARP1 activity assay was performed by Huawei Pharmaceutical Company (Jinan, China). The concentration required for 50% inhibition of PARP1 enzymatic activity (IC_{50}) was calculated using nonlinear regression with normalized dose response fit using Prism GraphPad software. Each well was precoated with histone (20 μ g/mL) diluted in 100 μ L of PBS buffer (contains 10 mmol/L NaH_2PO_4 , 10 mmol/L Na_2HPO_4 , 150 mmol/L NaCl, pH 7.4) by incubation at 4 °C overnight. 25 μ mol/L of biotinylated NAD⁺, 200 nmol/L of sDNA and

100 $\mu\text{mol/L}$ of NAD^+ diluted in 30 μL of reaction buffer (contains 2 mmol/L MgCl_2 and 50 mmol/L Tris, pH 8.0) were added into each well, and then 5 μL of solvent control or compound was added at varying concentrations. The reaction was initiated by the addition of 20 μL of PARP (50 ng/well) at 30 $^\circ\text{C}$ for 60 min. Then the reaction solution was added 50 μL streptavidin conjugated HRP. The assay was performed at 30 $^\circ\text{C}$ for additional 0.5 h. Finally, 100 μL of solution (contains luminol and H_2O_2 in 0.1 mol/L citrate buffer, pH 5.4) was added and luminescent signal was measured using Molecular Devices Spectra Max M5 microplate reader (a multi well spectrophotometer, San Jose, CA, USA).

4.5.2. BRD4 inhibition assays

The assay was performed by time-resolved fluorescence resonance energy transfer (TR-FRET) technology using a recombinant BRD4(BD1 + BD2) and its corresponding ligand (BET). The BRD4 activity assay was performed by Huawei Pharmaceutical Company. The TR-FRET binding from the assay was correlated with the amount of ligand binding to the bromodomain. The 20 μL reaction mixture in assay buffer contains either bromodomains, BET ligand and the indicated amount of inhibitor. For the negative control (blank), 5 μL of the assay buffer was added instead of the BET ligand. The reaction mixture incubated for 2 h. After the incubation with the ligand, TR-FRET signal was measured by using Tecan Infinite M1000 plate reader (Männedorf, Switzerland). The compounds final concentration of DMSO was 1% in all reactions. All of the binding reactions were conducted at room temperature.

4.5.3. Cell culture and reagent

All the cell lines used in this study were purchased from American Type Culture Collection (ATCC, Manassas, VA, USA). MDA-MB-231, MDA-MB-468 and MCF-7 cells were cultured in Dulbecco Modified Eagle Medium (DMEM) supplemented with 10% fetal bovine serum and incubated with 5% CO_2 . Primary antibodies against BRD4 (#13440), c-Myc (#5605), PARP (#9532), BAX (#5023), BCL-2 (#2870), caspase-3 (#9662), were purchased from Cell Signaling Technologies (Boston, MA, USA). PAR (#ab14459) was purchased from Abcam (Cambridge, UK). MTT (#M2128) was purchased from Sigma–Aldrich (St. Louis, MO, USA).

4.5.4. Cell viability assay

Cells were dispensed in 96-well plates at a density of 5.5×10^4 cells/mL. After 24 h incubation, cells were treated with different concentrations of synthetic compounds for the indicated time periods. Cell viability was measured by the MTT assay.

4.5.5. Flow cytometric analysis

For Annexin V-FITC/PI staining, the treated cells were collected, washed twice with PBS and then stained with Annexin V-FITC (1:1000) in binding buffer at room temperature in the dark. 15 min later, the cells were incubated with PI staining solution for 5 min. Then the cells were measured by flow cytometry (Becton Dickinson, CA, USA).

4.5.6. The cell cycle analysis

The cell cycle analysis was performed with cells seeded in 6-well plates (3×10^3 cells/well) in growth media. The cells were allowed to attach overnight. The cultures were treated by different concentration of **19d** with 0, 1, 3.3 or 10 $\mu\text{mol/L}$. The collected

cells were then washed in PBS and fixed in 95% ethanol. The cells were stained with 50 $\mu\text{g/mL}$ PI containing 10 $\mu\text{g/mL}$ RNase A and then analyzed in fluorescence activated cell sorting. The percentages of cells in the G1, S, and G2/M phases were determined.

4.5.7. Colony formation assay

The colony formation assay was performed with cells seeded in 6-well plates (500 cells/well). After 2 weeks, cells were fixed with methanol and stained with crystal violet. The number of colonies was counted. Data represent the means \pm SD from 3 independent experiments performed in triplicate wells.

4.5.8. Western blot analysis

Western blot analysis was carried out by the following method. Cells were treated with compound **19d**, RVX-208, Olaparib and SBI0206965 for indicated times. Then both adherent and floating cells were collected, which was added with a Rapa buffer with protease inhibitor and phosphatase inhibitor cocktail (Sigma–Aldrich) after centrifugation ($12,000 \times g$ at 4 $^\circ\text{C}$ for 15 min). The protein concentration was determined using the bicinchoninic acid method. Proteins were separated by sodium dodecyl sulphate-polyacrylamide gel electrophoresis and transferred to nitrocellulose membranes. The membranes were blocked with Tris buffered saline with Tween-20 (TBST) containing 5% skimmed milk at room temperature for 1 h, incubated overnight with primary antibodies at 4 $^\circ\text{C}$, and subsequently incubated with secondary horseradish peroxidase conjugated, goat anti-rabbit or goat anti-mouse IgG (Abcam) at room temperature for 1 h, then visualized by using ECL reagents.

4.5.9. Pharmacokinetic studies of compound 19d

The pharmacokinetic analysis of compound **19d** was conducted in three male Sprague–Dawley rats. The animal studies were conducted in conformity with institutional guide for the care and use of laboratory animals, and all animal protocols were approved by the Animal Ethics Committee of Sichuan University (Chengdu, China). All experiments with animals were in accordance with the animal care and use guidelines. The group of three rats were administered the agent orally. The group was orally administered at a dose of 10 mg/kg with a dosing volume of 10 mL/kg for rats. The blood samples were collected were collected at 0.25, 0.5, 1, 2, 4, 6, 8, and 24 h. Blood were collected for plasma study. The saline solutions were formulated in 4% DMSO and 10% solution of HS-15. Briefly, the animals were restrained manually at the designated time points. Approx. 200 μL of blood were taken from the animals *via* the jugular vein into heparin sodium tubes. Blood samples were put on ice and centrifuged to obtain plasma samples ($6800 \times g$, 6 min under 4 $^\circ\text{C}$) within 2 h. The concentrations of the compound in the plasma were analyzed using liquid chromatography–mass spectrometry (LC–MS/MS) after protein precipitation. The concentration–time data of plasma compound **19d** were analyzed to derive the pharmacokinetic parameters. Fasted overnight with metabolism cages and fed 4 h after administration, freed access to water. Plasma samples were stored at approximately -80 $^\circ\text{C}$ until analysis.

4.5.10. Xenograft breast cancer models

Forty female nude mice (BALB/c, 6–8 weeks, 15–17 g) were injected subcutaneously with MCF-7 cells (5×10^6 cells/mouse), another 40 female nude mice were injected subcutaneously with MDA-MB-468 cells (5×10^6 cells/mouse). When the tumors reached 100 mm^3 in volume ($V = L \times W^2/2$), 40 mice were

divided into four groups ($n = 10$) for each cell line, respectively. Three groups were treated with different doses of **19d** (low dose, 20 mg/kg; median dose, 40 mg/kg; high dose, 80 mg/kg) once a day by intragastric administration for 20 or 18 days, whereas the control group was treated with vehicle control. During the treatment, the tumor volumes and body weight were measured every 3 days until the end of the study. At the end of treatment, all mice were sacrificed. The tumor tissues were harvested and weighed. Then, the tumor tissues were frozen in liquid nitrogen or fixed in formalin immediately.

4.5.11. IHC assay

The fixed tissue was dehydrated by a fully automatic dehydrator, embedded, and sliced as follows: the dewaxed slice was placed in a dyeing tank (3% methanol, hydrogen peroxide) at room temperature for 10 min. Washed 3 times with PBS, each time for 5 min, then immersed the section in 0.01 mol/L citrate buffer (pH 6.0). After heating, the fire was turned off after boiling, and repeated once time after 5 min. Continued to wash with the PBS twice for 5 min each time; added goat serum blocking solution at room temperature for 20 min; added antibody, overnight at 4 °C; added antibody, and stored at 37 °C for 30 min; washed 3 times with PBS, each time for 5 min; DAB color development: using the DAB color development kit (Beijing Zhongshan Jinqiao Biotechnology Co., Ltd., Beijing, China), mixed the reagent and added it to the slice. Colored development at room temperature, mirror control time was usually about 2 min, washed with distilled water; lightly counterstain with hematoxylin, dehydrated, transparent, and sealed with neutral gum. The above specimens were all performed according to the pathological examination standard operation process (SOP) procedure. The images acquisition of the slice was performed using the BA200 Digital trinocular camera micro-camera system produced by McAudi Industrial Group Co., Ltd. (Xiamen, China). Each section was observed at 100 times before the whole tissue, and then 3 fields were selected to collect 400 times of microscopic images.

4.5.12. HE staining assay

The fixed tissues were dehydrated by the automatic dehydrator, embedded, and sliced as follows: the slice was dewaxed into water, the hematoxylin was stained for 10–20 min, and rinsed with tap water for 1–3 min; differentiated with hydrochloric acid and alcohol for 5–10 s; washed with tap water for 1–3 min, putted into warm water of 50 °C or weak alkaline solution until blue color appeared, then washed it with tap water for 1–3 min; put it into 85% alcohol for 3–5 min, dyed with eosin for 3–5 min, then washed with water for 3–5 s; dehydrated with different gradients of alcohol, used xylene to make it transparent, and finally sealed with neutral gum solid. The above specimens were all performed according to the pathological examination SOP procedure. The BA200 Digital trinocular camera micro-camera system was produced by McAudi Industrial Group Co., Ltd. (Xiamen, China), which was used to image the slices. Each slice was observed at 40 times before the whole tissue was observed. The gross lesions were observed, and the area was selected and collected 100 and 400 times picture to observe specific lesions.

4.5.13. Statistical analysis

The presented data and results were confirmed in at least 3 independent experiments. The data were expressed as means \pm SD and analyzed with GraphPad Prism 6.0. Statistical comparisons were made by 1-way ANOVA and Student's *t*-test of SPSS 17.0

(Chicago, IL, USA). $P < 0.05$ was considered statistically significant.

Acknowledgments

We are grateful for financial support from the National Natural Science Foundation of China (grant Nos. 81922064, 81874290 and 81673455 to Liang Ouyang, grant No. 81673455 to Bo Liu, grant Nos. 81573290 and U1603123 to Jie Liu) and project of Science and Technology Department of Sichuan Province (grant No. 20YYJC3921 to Jie Liu, China).

Author contributions

Liang Ouyang, Bo Liu and Jie Liu conceived the project and supervised the project. Xiaosa Chang and Kai Zhang carried out synthesis, purification, and characterization of target compounds. Dejuan Sun, Guan Wang, Yanmei Chen and Huidan Tan performed the biological experiments. Xiaosa Chang, Dejuan Sun and Danfeng Shi analyzed data and drafted the manuscript. Liang Ouyang, Bo Liu and Jie Liu revised the manuscript. All authors discussed the results and approved the final manuscript.

Conflicts of interest

The authors declare no competing financial interest.

Appendix A. Supporting information

Supporting data to this article can be found online at <https://doi.org/10.1016/j.apsb.2020.06.003>.

References

- Banerjee S, Reis-Filho JS, Ashley S, Steele D, Ashworth A, Lakhani SR, et al. Basal-like breast carcinomas: clinical outcome and response to chemotherapy. *J Clin Pathol* 2006;**59**:729–35.
- Chowdhury P, Nagesh PKB, Khan S, Hafeez BB, Chauhan SC, Jaggi M, et al. Development of polyvinylpyrrolidone/paclitaxel self-assemblies for breast cancer. *Acta Pharm Sin B* 2018;**8**:602–14.
- Shi Y, Jin J, Ji W, Guan X. Therapeutic landscape in mutational triple negative breast cancer. *Mol Canc* 2018;**17**:99.
- Khosravi-Shahi P, Cabezon-Gutiérrez L, Custodio-Cabello S. Metastatic triple negative breast cancer: optimizing treatment options, new and emerging targeted therapies. *Asia Pac J Clin Oncol* 2017;**14**:32–9.
- Zheng G, Hemminki A, Försti A, Sundquist J, Sundquist K, Hemminki K. Second primary cancer after female breast cancer: familial risks and cause of death. *Cancer Med* 2019;**8**:400–7.
- den Hollander P, Savage MI, Brown PH. Targeted therapy for breast cancer prevention. *Front Oncol* 2013;**3**:250.
- Mei D, Chen B, He B, Liu H, Lin Z, Lin J, et al. Actively priming autophagic cell death with novel transferrin receptor-targeted nanomedicine for synergistic chemotherapy against breast cancer. *Acta Pharm Sin B* 2019;**9**:1061–77.
- Odle TG. Precision medicine in breast cancer. *Radiol Technol* 2017;**88**:401–21.
- Rabindran SK, Discafani CM, Rosfjord EC, Baxter M, Floyd MB, Golas J, et al. Antitumor activity of HKI-272, an orally active, irreversible inhibitor of the HER-2 tyrosine kinase. *Cancer Res* 2004;**64**:3958–65.
- He P, Niu S, Wang S, Shi X, Feng S, Du L, et al. Discovery of WS-157 as a highly potent, selective and orally active EGFR inhibitor. *Acta Pharm Sin B* 2019;**9**:1193–203.

11. Corona SP, Generali D. Abemaciclib: a CDK4/6 inhibitor for the treatment of HR+/HER2– advanced breast cancer. *Drug Des Dev Ther* 2018;**12**:321–30.
12. Zhan P, Itoh Y, Suzuki T, Liu X. Strategies for the discovery of target-specific or isoform-selective modulators. *J Med Chem* 2015;**58**:7611–33.
13. Hamadeh IS, Patel JN, Rusin S, Tan AR. Personalizing aromatase inhibitor therapy in patients with breast cancer. *Canc Treat Rev* 2018;**70**:47–55.
14. Zhu G, Chen X. Aptamer-based targeted therapy. *Adv Drug Deliv Rev* 2018;**134**:65–78.
15. Murali R, Grisham RN, Soslow RA. The roles of pathology in targeted therapy of women with gynecologic cancers. *Gynecol Oncol* 2018;**148**:213–21.
16. Fong PC, Boss DS, Yap TA, Tutt A, Wu P, Mergui-Roelvink M, et al. Inhibition of poly(ADP-ribose) polymerase in tumors from *BRCA* mutation carriers. *N Engl J Med* 2009;**361**:123–34.
17. Bitler BG, Watson ZL, Wheeler LJ, Behbakht K. PARP inhibitors: clinical utility and possibilities of overcoming resistance. *Gynecol Oncol* 2017;**147**:695–704.
18. McCann KE, Hurvitz SA. Advances in the use of PARP inhibitor therapy for breast cancer. *Drugs Context* 2018;**7**:212540.
19. JJJ Geenen, Linn SC, Beijnen JH, Schellens JHM. PARP inhibitors in the treatment of triple-negative breast cancer. *Clin Pharmacokinet* 2018;**57**:427–37.
20. Mirza MR, Pignata S, Ledermann JA. Latest clinical evidence and further development of PARP inhibitors in ovarian cancer. *Ann Oncol* 2018;**29**:1366–76.
21. Magen A, Das Sahu A, Lee JS, Sharmin M, Lugo A, Gutkind JS, et al. Beyond synthetic lethality: charting the landscape of pairwise gene expression states associated with survival in cancer. *Cell Rep* 2019;**28**:938–48.
22. Xiang H, Zhang J, Lin C, Zhang L, Liu B, Ouyang L. Targeting autophagy-related protein kinases for potential therapeutic purpose. *Acta Pharm Sin B* 2020;**10**:569–81.
23. Bryant HE, Schultz N, Thomas HD, Parker KM, Flower D, Lopez E, et al. Specific killing of *BRCA2*-deficient tumours with inhibitors of poly(ADP-ribose) polymerase. *Nature* 2005;**434**:913–7.
24. Farmer H, McCabe N, Lord CJ, Tutt AN, Johnson DA, Richardson TB, et al. Targeting the DNA repair defect in *BRCA* mutant cells as a therapeutic strategy. *Nature* 2005;**434**:917–21.
25. Mateo J, Lord CJ, Serra V, Tutt A, Balmaña J, Castroviejo-Bermejo M, et al. A decade of clinical development of PARP inhibitors in perspective. *Ann Oncol* 2019;**30**:1437–47.
26. Kamel D, Gray C, Walia JS, Kumar V. PARP inhibitor drugs in the treatment of breast, ovarian, prostate and pancreatic cancers: an update of clinical trials. *Curr Drug Targets* 2018;**19**:21–37.
27. Papeo G, Posteri H, Borghi D, Busel AA, Caprera F, Casale E, et al. Discovery of 2-[1-(4,4-difluorocyclohexyl) piperidin-4-yl]-6-fluoro-3-oxo-2,3-dihydro-1*H*-isoindole-4-carboxamide (NMS-P118): a potent, orally available, and highly selective PARP-1 inhibitor for cancer therapy. *J Med Chem* 2015;**58**:6875–98.
28. Li L, Karanika S, Yang G, Wang J, Park S, Broom BM, et al. Androgen receptor inhibitor-induced “*BRCAness*” and PARP inhibition are synthetically lethal for castration-resistant prostate cancer. *Sci Signal* 2017;**10**:480.
29. Zhang B, Lyu J, Yang EJ, Liu Y, Wu C, Pardeshi L, et al. Class I histone deacetylase inhibition is synthetic lethal with *BRCA1* deficiency in breast cancer cells. *Acta Pharm Sin B* 2020;**10**:615–27.
30. De P, Sun Y, Carlson JH, Friedman LS, Leyland-Jones BR, Dey N. Doubling down on the PI3K-AKT-mTOR pathway enhances the antitumor efficacy of PARP inhibitor in triple negative breast cancer model beyond *BRCA-ness*. *Neoplasia* 2014;**16**:43–72.
31. O’Neil NJ, Bailey ML, Hieter P. Synthetic lethality and cancer. *Nat Rev Genet* 2017;**18**:613–23.
32. Yap TA, Plummer R, Azad NS, Helleday T. The DNA damaging revolution: PARP inhibitors and beyond. *Am Soc Clin Oncol Educ Book* 2019;**39**:185–95.
33. Berger NA, Besson VC, Boulares AH, Bürkle A, Chiarugi A, Clark RS, et al. Opportunities for the repurposing of PARP inhibitors for the therapy of non-oncological diseases. *Br J Pharmacol* 2018;**175**:192–222.
34. Lord CJ, Ashworth A. PARP inhibitors: synthetic lethality in the clinic. *Science* 2017;**355**:1152–8.
35. Mengwasser KE, Adeyemi RO, Leng Y, Choi MY, Clairmont C, D’Andrea AD, et al. Genetic screens reveal *FEN1* and *APEX2* as *BRCA2* synthetic lethal targets. *Mol Cell* 2019;**73**:885–99.
36. Smith I, Greenside PG, Natoli T, Lahr DL, Wadden D, Tirosh I, et al. Evaluation of RNAi and CRISPR technologies by large-scale gene expression profiling in the Connectivity Map. *PLoS Biol* 2017;**15**:e2003213.
37. Zuber J, Shi J, Wang E, Rappaport AR, Herrmann H, Sison EA, et al. RNAi screen identifies Brd 4 as a therapeutic target in acute myeloid leukaemia. *Nature* 2011;**478**:524–8.
38. Sun C, Yin J, Fang Y, Chen J, Jeong KJ, Chen X, et al. BRD4 inhibition is synthetic lethal with PARP inhibitors through the induction of homologous recombination deficiency. *Canc Cell* 2018;**33**:401–16.
39. Karakashev S, Zhu H, Yokoyama Y, Zhao B, Fatkhutdinov N, Kossenkov AV, et al. BET bromodomain inhibition synergizes with PARP inhibitor in epithelial ovarian cancer. *Cell Rep* 2017;**21**:3398–405.
40. Stanlie A, Yousif AS, Akiyama H, Honjo T, Begum NA. Chromatin reader Brd 4 functions in Ig class switching as a repair complex adaptor of nonhomologous end-joining. *Mol Cell* 2014;**55**:97–110.
41. Li X, Baek G, Ramanand SG, Sharp A, Gao Y, Yuan W, et al. BRD4 promotes DNA repair and mediates the formation of *TMPRSS2-ERG* gene rearrangements in prostate cancer. *Cell Rep* 2018;**22**:796–808.
42. Filippakopoulos P, Knapp S. Targeting bromodomains: epigenetic readers of lysine acetylation. *Nat Rev Drug Discov* 2014;**13**:337–56.
43. Miller AL, Fehling SC, Garcia PL, Gamblin TL, Council LN, van Waardenburg RCAM, et al. The BET inhibitor JQ1 attenuates double-strand break repair and sensitizes models of pancreatic ductal adenocarcinoma to PARP inhibitors. *EBioMedicine* 2019;**44**:419–30.
44. Sun C, Yin J, Fang Y, Chen J, Jeong KJ, Chen X, et al. Rational combination therapy with PARP and BRD4 inhibitor in ovarian cancer. *Clin Canc Res* 2018;**24**:42.
45. He S, Dong G, Wu S, Fang K, Miao Z, Wang W, et al. Small molecules simultaneously inhibiting p53-murine double minute 2 (MDM2) interaction and histone deacetylases (HDACs): discovery of novel multitargeting antitumor agents. *J Med Chem* 2018;**61**:7245–60.
46. Chang Y, Lu X, Shibu MA, Dai YB, Luo J, Zhang Y, et al. Structure based design of *N*-(3-((1*H*-pyrazolo[3,4-*b*]pyridin-5-yl)ethynyl)benzenesulfonamides as selective leucine-zipper and sterile- α motif kinase (ZAK) inhibitors. *J Med Chem* 2017;**60**:5927–32.
47. Du J, Guo J, Kang D, Li Z, Wang G, Wu J, et al. New techniques and strategies in drug discovery. *Chin Chem Lett* 2020;**31**:1695–708.
48. Sun D, Zhao Y, Zhang S, Zhang L, Liu B, Ouyang L. Dual-target kinase drug design: current strategies and future directions in cancer therapy. *Eur J Med Chem* 2020;**188**:112025.
49. Li Z, Ding L, Li Z, Wang Z, Suo F, Shen D, et al. Development of the triazole-fused pyrimidine derivatives as highly potent and reversible inhibitors of histone lysine specific demethylase 1 (LSD1/KDM1A). *Acta Pharm Sin B* 2019;**9**:794–808.
50. Price AJ, Howard S, Cons BD. Fragment-based drug discovery and its application to challenging drug targets. *Essays Biochem* 2017;**61**:475–84.
51. Pathan AA, Panthi B, Khan Z, Koppula PR, Alanazi MS, Sachchidanand, et al. Lead identification for the K-Ras protein: virtual screening and combinatorial fragment-based approaches. *Oncotargets Ther* 2016;**9**:2575–84.
52. Joshi P, Chia S, Habchi J, Knowles TP, Dobson CM, Vendruscolo M. A fragment-based method of creating small-molecule libraries to target the aggregation of intrinsically disordered proteins. *ACS Comb Sci* 2016;**18**:144–53.

53. Wu SY, Chiang CM. The double bromodomain-containing chromatin adaptor Brd 4 and transcriptional regulation. *J Biol Chem* 2007;**282**: 13141–5.
54. Vollmuth F, Blankenfeldt W, Geyer M. Structures of the dual bromodomains of the P-TEFb-activating protein Brd 4 at atomic resolution. *J Biol Chem* 2009;**284**:36547–56.
55. Filippakopoulos P, Picaud S, Mangos M, Keates T, Lambert JP, Barsyte-Lovejoy D, et al. Histone recognition and large-scale structural analysis of the human bromodomain family. *Cell* 2012;**149**: 214–31.
56. Shi J, Wang Y, Zeng L, Wu Y, Deng J, Zhang Q, et al. Disrupting the interaction of BRD4 with diacetylated twist suppresses tumorigenesis in basal-like breast cancer. *Canc Cell* 2014;**25**:210–25.
57. Faivre EJ, McDaniel KF, Albert DH, Mantena SR, Plotnik JP, Wilcox D, et al. Selective inhibition of the BD2 bromodomain of BET proteins in prostate cancer. *Nature* 2020;**578**:306–10.
58. Gilan O, Rioja I, Knezevic K, Bell MJ, Yeung MM, Harker NR, et al. Selective targeting of BD1 and BD2 of the BET proteins in cancer and immunoinflammation. *Science* 2020;**368**:387–94.
59. Liu S, Yosief HO, Dai L, Huang H, Dhawan G, Zhang X, et al. Structure-guided design and development of potent and selective dual bromodomain 4 (BRD4)/polo-like kinase 1 (PLK1) inhibitors. *J Med Chem* 2018;**61**:7785–95.
60. Watts E, Heidenreich D, Tucker E, Raab M, Strebhardt K, Chesler L, et al. Designing dual inhibitors of anaplastic lymphoma kinase (ALK) and bromodomain-4 (BRD4) by tuning kinase selectivity. *J Med Chem* 2019;**62**:2618–37.
61. Cheng G, Wang Z, Yang J, Bao Y, Xu Q, Zhao L, et al. Design, synthesis and biological evaluation of novel indole derivatives as potential HDAC/BRD4 dual inhibitors and anti-leukemia agents. *Bioorg Chem* 2019;**84**:410–7.
62. Schütz M, Bouchet A, Chiavarino B, Crestoni ME, Fornarini S, Dopfer O. Effects of aromatic fluorine substitution on protonated neurotransmitters: the case of 2-phenylethylamine. *Chemistry* 2016; **22**:8124–36.
63. Meanwell NA. Fluorine and fluorinated motifs in the design and application of bioisosteres for drug design. *J Med Chem* 2018;**61**: 5822–80.
64. Mei H, Han J, Fustero S, Medio-Simon M, Sedgwick DM, Santi C, et al. Fluorine-containing drugs approved by the FDA in 2018. *Chemistry* 2019;**25**:11797–819.
65. Mio C, Gerratana L, Bolis M, Caponnetto F, Zanello A, Barbina M, et al. BET proteins regulate homologous recombination-mediated DNA repair: BRCAness and implications for cancer therapy. *Int J Canc* 2019;**144**:755–66.
66. Yang L, Zhang Y, Shan W, Hu Z, Yuan J, Pi J. Repression of BET activity sensitizes homologous recombination-proficient cancers to PARP inhibition. *Sci Transl Med* 2017;**9**:eaal1645.
67. Fu L, Wang S, Wang X, Wang P, Zheng Y, Yao D, et al. Crystal structure-based discovery of a novel synthesized PARP1 inhibitor full or (OL-1) with apoptosis-inducing mechanisms in triple-negative breast cancer. *Sci Rep* 2016;**6**:3.
68. Liu S, Li F, Pan L, Yang Z, Shu Y, Lv W, et al. BRD4 inhibitor and histone deacetylase inhibitor synergistically inhibit the proliferation of gallbladder cancer *in vitro* and *in vivo*. *Canc Sci* 2019;**110**:2493–506.
69. Ouyang L, Zhang L, Liu J, Fu L, Yao D, Zhao Y, et al. Discovery of a small-molecule bromodomain-containing protein 4 (BRD4) inhibitor that induces AMP-activated protein kinase-modulated autophagy-associated cell death in breast cancer. *J Med Chem* 2017;**60**: 9990–10012.
70. Li F, Liu Z, Sun H, Li C, Wang W, Ye L, et al. PCC0208017, a novel small-molecule inhibitor of MARK3/MARK4, suppresses glioma progression *in vitro* and *in vivo*. *Acta Pharm Sin B* 2020;**10**:289–300.
71. Tang Z, Li C, Kang B, Gao G, Li C, Zhang Z. GEPIA: a web server for cancer and normal gene expression profiling and interactive analyses. *Nucleic Acids Res* 2017;**45**:98–102.
72. Xing J, Lu W, Liu R, Wang Y, Xie Y, Zhang H, et al. Machine-learning-assisted approach for discovering novel inhibitors targeting bromodomain-containing protein 4. *J Chem Inf Model* 2017;**57**: 1677–90.